minerals

MDPI

Article

Indium Mineralization in the Xianghualing Sn-Polymetallic Orefield in Southern Hunan, Southern China

Jianping Liu [1,2], Yanan Rong [1,2], Shugen Zhang [1,2], Zhongfa Liu [1,2,*] and Weikang Chen [1,2]

[1] Key Laboratory of Metallogenic Prediction of Nonferrous Metals and Geological Environment Monitoring (Central South University), Ministry of Education, Changsha 410083, China; liujianping@csu.edu.cn (J.L.); rongyn19@163.com (Y.R.); zhangshugenzsg@163.com (S.Z.); 18777398186@163.com (W.C.)

[2] School of Geosciences and Info-Physics, Central South University, Changsha 410083, China

* Correspondence: liuzf61521@csu.edu.cn; Tel.: +86-731-888-30616

Received: 28 July 2017; Accepted: 15 September 2017; Published: 18 September 2017

Abstract: Although numerous W–Sn–Pb–Zn polymetallic deposits are located in southern Hunan, and In-bearing deposits are related to W–Sn–Pb–Zn polymetallic deposits, Indium mineralization in southern Hunan is poorly studied. In order to investigate the In mineralization of the Xianghualing orefield, which is a typical orefield in southern Hunan, ore bulk chemistry, microscopic observation, and electron-probe microanalysis of vein-type (type-I) and porphyry-type (type-II) Sn–Pb–Zn orebodies were studied. The In contents of the type-I orebodies varies from 0.79 to 1680 ppm (avg. 217 ppm, $n = 29$), and that of the type-II orebodies varies from 10 to 150 ppm (avg. 64 ppm, $n = 10$). Although chalcopyrite and stannite contain trace amounts of In, sphalerite is the most important In-rich mineral in the orefield. Sphalerite in type-I orebodies contains from <0.02 to 21.96 wt % In, and in type-II orebodies contains from <0.02 to 0.39 wt % In. Indium-rich chemical-zoned sphalerite contains 7 to 8 wt % In in its core and up to 21.96 wt % In in its rim. This sphalerite may be the highest In-bearing variety in Southern China. The Cd contents of the In-rich sphalerite ranges from 0.35 to 0.45 wt %, which places it in the the "Indium window" of the Cu–In–S phases. The geological and structural features of the Xianghualing orefield indicate that the In mineralization of the two types of In-bearing Sn–Pb–Zn orebodies is related to the volatile-rich, In-rich, A-type granites, and is controlled by the normal faults of magmatic-diapiric activity extensional features.

Keywords: indium; In-bearing sphalerite; Sn-polymetallic deposits; Xianghualing orefield; southern China

1. Introduction

Indium is a dispersed scarce element with a low abundance of 0.05 ppm in the Earth's crust [1]. Indium alloys are widely used in high-tech applications, e.g., flat-panel displays, solders, semiconductor materials, and photovoltaic solar cells [2]. Due to the demand for flat panel displays and photovoltaic solar cells, indium has become a high-priced commodity and is regarded as a critical and strategic mineral resource by many governments and organizations [3].

The geology and mineralogy of In-bearing deposits were studied during the last decade [4,5]. Major In deposits or mineralization regions have been identified throughout the world, such as Mount Pleasant in Canada [6–8], southwestern Bolivia [4,9], southern Finland and adjacent areas [10–12], southwestern England [13], the eastern Erzgebirge in Germany [14], the Iberian Pyrite Belt [15,16], Japanese Arc [5,17], the Southern Dahinggang Mountains in northern China [18,19], and southern China [20–24]. Two types of primary, industrial In-bearing deposits have been identified: (1) volcanic-hosted massive sulfide deposits, e.g., Kidd Creek in Canada and Neves Corvo in

Portugal [4]; and (2) vein-type, disseminated-type, and skarn-type deposits in granitic terranes [5]. Indium-bearing polymetallic vein-type deposits are generally structurally controlled and occur within faults systems [4]. These types of deposits are widely distributed around the world and are the most important In producing deposits [4], e.g., the Tosham deposits in Japan [5], the Bolivian Sn-polymetallic deposits [9], and the Dajing deposit in Northern China [19].

Southern China is one of the richest In mineralization areas in the world [20]. Indium-bearing deposits are distributed in the Yunan, Guangxi, Guangdong, and Hunan provinces (Figure 1a). Major In deposits in southern China occur in the western section of South China; e.g., the Dachang and Dulong deposits. Few In deposits occur in the eastern section; e.g., the Nanling metallogenetic belt [24]. The southern Hunan district is the area with the most W–Sn–Pb–Zn mineralization in the Nanling metallogenetic belt [24,25]. The Huangshaping, Xianghualing, and Yejiwei deposits (Figure 1b) in southern Hunan are also reported to contain In [5,26,27]. In-rich sphalerite (9–10 wt % In) was discovered in the Yejiwei deposit [24]. Furthermore, the southern Hunan district is located in the NE-trending North Guangxi–South Hunan A-type granite belt [28,29], which is related to In-bearing deposits [6,7,10]. Thus, the southern Hunan district is an important In mineralization and exploration area in southern China.

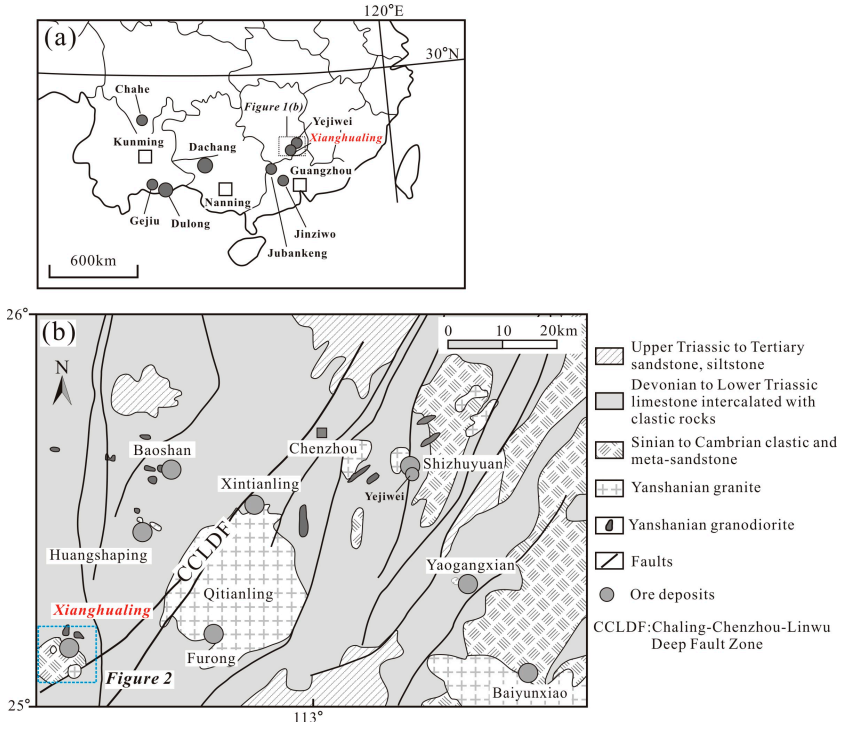

Figure 1. (**a**) Distribution of major In-bearing base metal deposits in southern China (after Ref. [20]), showing the location of the Xianghualing Orefield in southern Hunan; (**b**) simplified regional geologic map of southern Hunan, showing the important W–Sn–Pb–Zn deposits (after Ref. [30]).

The Xianghualing Orefield is a typical Sn-ploymetallic orefield in southern Hunan. The orefield contains many types of deposits including granite-type Nb–Ta, skarn-type W–Sn–Be, vein-type Sn–Pb–Zn, and porphyry-type Sn–Pb–Zn deposits. According to previous studies [27], this orefield also hosts In-bearing ores, e.g., 15–52 ppm In in the Xinfeng deposit and 20–60 ppm In in the Paojinshan deposit [27]. Therefore, the Xianghualing Orefield is a good deposit for the investigation of In mineralization in southern Hunan. In order to characterize the In metallogeny of the Xianghualing orefield, ore bulk geochemistry, ore petrology, and electron-probe microanalyses (EPMA) of the In-bearing minerals in the vein-type (type-I) and porphyry-type (type-II) Sn–Pb–Zn orebodies were studied, and In genesis is investigated and discussed in this paper.

2. Geologic Setting

The Xianghualing orefield is located in the southwestern corner of the southern Hunan metallogenetic belt (Figure 1b). The outcropping strata in the belt consists of Sinian to Cambrian low-grade metamorphic rocks, Devonian to Lower Triassic limestone intercalated with clastic rocks, and Upper Triassic to Tertiary sandstone and siltstone. The Yangshanian granites intrude extensively in southern Hunan with the largest being the Qitianling intrusion [31–33], and they control the formation of a number of large-scale porphyry, skarn, and vein-type W–Sn–Pb–Zn deposits (Figure 1b), e.g., the Shizhuyuan [34], Baoshan [35], Huangshaping [36–38], Xianghualing [39], Xintianling [35], Yaoganxiang [30], Baiyunxian, and Furong deposits [35,40].

2.1. Geology of the Xianghualing Orefield

2.1.1. Stratigraphy and Structural Geology

The rocks of the Xianghualing orefield include Cambrian metamorphic rocks, Devonian–Permian carbonate–clastic rocks, Cretaceous red sandstones, and Quaternary covers (Figure 2). The Cambrian and mid-Devonian Tiaomajian, Qiziqiao, and ShetianqiaofFormations are the host rocks of the ore deposits in the Xianghualing Orefield [41]. The Cambrian rocks are composed mainly of low-grade metamorphic rocks, slate and phyllite, which are located in the central part of the orefield, and contain quartz-vein-type W deposits [27,42]. The Tiaomajian formation consists of neritic-littoral marine clastic rocks [41]. The Qiziqiao and Shetianqiao formations consist of shallow-marine carbonate rocks, which are the host rocks of the Sn–Pb–Zn orebodies.

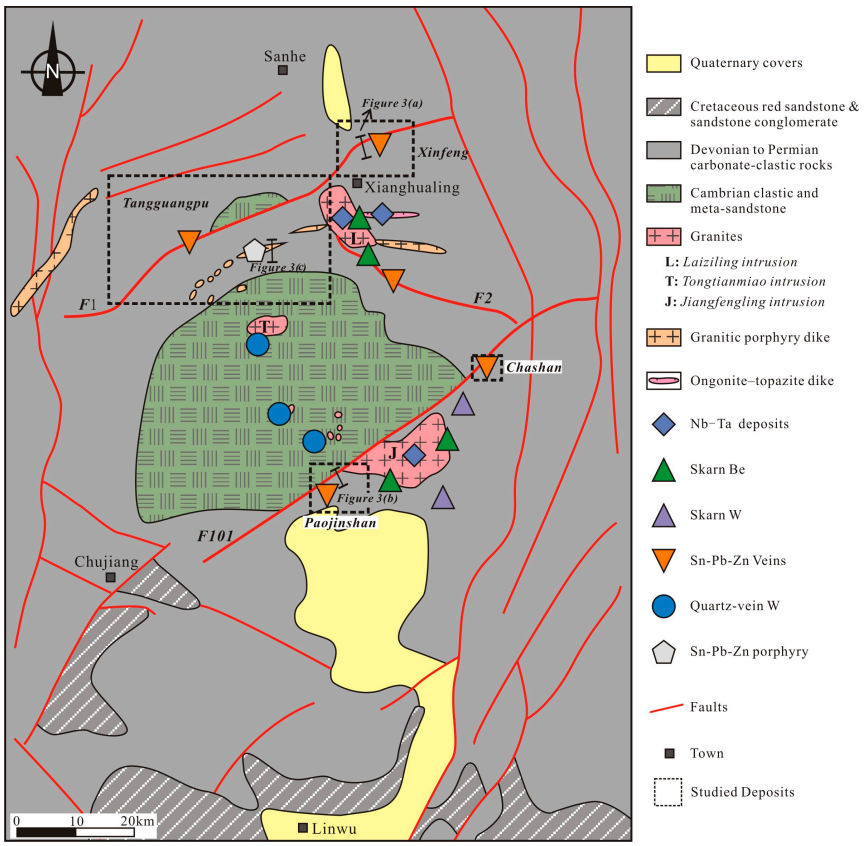

Figure 2. Geologic map of the Xianghualing Orefield (after Ref. [15]), showing the distribution of the primary rare metals and W–Sn–Pb–Zn deposits and the four studied deposits (the Xinfeng, Tangguanpu, Chashan, and Paojinshan Sn–Pb–Zn deposits).

The Xianghualing orefield is located in the Tongtianmiao Dome, the core of which is composed of Cambrian rocks and is surrounded by Devonian, carboniferous, and Permian rocks (Figure 2). The dome contains NS and NE trending faults as well as a few NW trending faults (Figure 2). The NE trending F_1, and F_{101} faults and the NW trending F_2 fault are the main faults controlling the development of vein-type orebodies [27] (Figure 2).

2.1.2. Intrusive Rocks

Granitic intrusions are common and occur as stocks and dikes in the orefield. Three large intrusions (from north to south) are the Laiziling, Tongtianmiao, and Jianfengling intrusions, which cover 0.3–4.4 km^2 [27,43]. These intrusions are highly differentiated granites including biotite granite, albite granite, and ongonite [44]. The Laiziling intrusion zonation pattern is zoned from bottom to top from biotite granite, to leucogranite to albite granite. Since all of the feldspar is being alkali feldspar, the granites are categorized as alkali-feldspar granites on the quartz–alkali feldspar–plagioclase (QAP) classification diagram [45,46]. Geochemically, the granites are high silica (SiO_2 = 70.36–75.52 wt %), alkali ($K_2O + Na_2O$ = 5.25–10.69 wt %), and are F-enriched (0.85–1.60 wt %) with molar $Al_2O_3/(CaO + Na_2O + K_2O)$ ratios (A/CNK) range of 0.97 to 3.70 (mostly > 1.1). According to these geochemical characteristics, the biotite granite is an A-type granite [43].

The felsic dikes consist of granitic porphyry, ongonite, and lamprophyre that are distributed around the Laiziling intrusion (Figure 2). The ongonite dike, which is 1770 m long and 1.8–18 m wide, is Nb and Ta enriched (Figure 2) and is located to the east of the Laiziling intrusion. The EW trending granitic porphyry dikes are located to the west of the Laiziling intrusion hosted Sn–Pb–Zn mineralization and form porphyry-type orebodies [41].

U–Pb zircon ages of the Laiziling, Jianfengling stocks and felsic dikes indicate that they were formed 155–150 Ma [33,43,46], which is consistent with the ages of granites in the Nanling region (160–150 Ma) [33].

2.1.3. Mineralization Type of the Xianghualing Orefield

Rare metal deposits and Sn–Pb–Zn deposits are located in the Xianghualing orefield and include (1) granite-type Nb–Ta deposits and an ongonite-type Nb–Ta deposit; (2) skarn-type Be deposits; (3) skarn-type scheelite deposits; (4) quartz-vein-type wolframite deposits; (5) vein-type Sn–Pb–Zn deposits hosted in faults; and (6) porphyry-type Sn–Pb–Zn deposits in granitic porphyry dikes [27].

Indium is always hosted within sulfides in these deposits [4,47]. The first four types of deposits listed above contain little sulfide and are not economic In-rich deposits. The last two types contain abundant sulfides and are mainly In-rich deposits. Furthermore, the last two types, especially vein-types, are the deposits most exploited in the Xianghualing orefield.

Vein-Type Sn–Pb–Zn Orebodies (Type-I)

The type-I orebodies, which are the most economic orebodies in the Xianghualing orefield, are distributed along faults F_1 and F_{101} as well as suborder faults (Figure 2). The Xinfeng and Tangguanpu deposits are hosted in the F_1 fault zone in the north, and the Chashan and Paojinshan deposits are hosted in the F_{101} fault zone in the south (Figure 2). The main orebodies of this type always occur within primary faults, while the secondary of this type of orebodies are hosted in suborder faults, e.g., the Xinfeng deposit (Figure 3a) and the Paojinshan deposit (Figure 3b). The size of the smaller orebodies is <200 m along strike, and that of larger orebodies is >1000 m. The type-I orebodies are 0.5–11 m thick with an average thickness of 2–3 m and extend more than 100–300 m along dips [27]. The chemical composition of the orebodies varies base on locations, with Pb–Zn consistently dominatinges in shallower orebodies, Pb–Zn–Sn to and Sn–Pb–Zn dominatinge in intermediate depth orebodies, and dominant Sn dominating in deeper orebodies [48]. The ore grade varies with an average of 0.66–1.72 wt % Sn, 1.14–3.03 wt % Pb, and 1.94–5.24 wt % Zn [27]. The Pb–Zn ores in the shallower orebodies contain 3.34–8.94 wt % Pb and 4.56–12.34 wt % Zn [27].

Porphyry-Type Sn–Pb–Zn Orebodies (Type-II)

Ten granitic porphyry dikes, including two large dikes (No. I & II), are distributed located in the Tangguanpu deposit in the northern part of the orefield. All of the granitic porphyry dikes have Sn–Pb–Zn mineralization. Dike No. I is 760 m long and 5–13 m (avg. 4.5 m) wide, strikes E–W, and dips 65°–85° S. The average ore grade of dike No. I is 0.33 wt % Sn, 1.20 wt % Pb, and 0.52 wt % Zn. Dike No. II is 1850 m in length, 1.05–18.92 m in width (avg. 7.94 m) [27], and dips 45–75° SW (Figure 3c) [49]. The average ore grade of dikes No. II is 0.42 wt % Sn, 1.02 wt % Pb, and 1.54 wt % Zn [27].

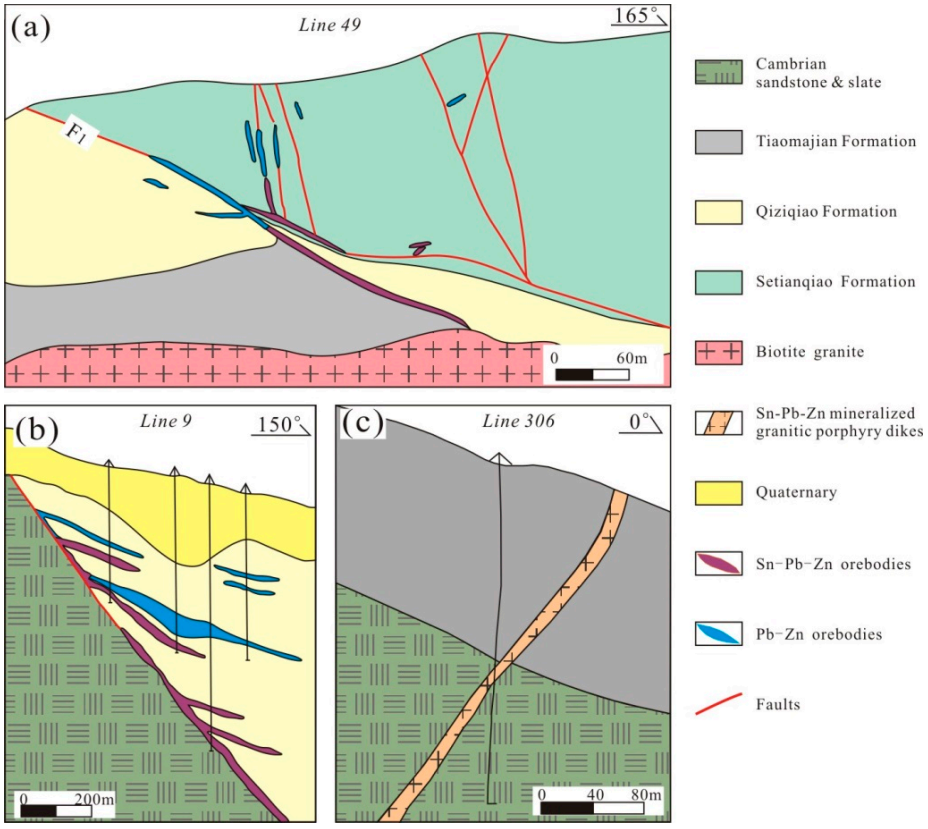

Figure 3. (**a**) Cross section of Line 49 in the Xinfeng deposit (after Ref. [50]), (**b**) cross section of Line 9 in the Paojinshan deposit (after Ref. [51]), showing the occurrence of type-I orebodies, and (**c**) cross section of Line 306 in the Tangguanpu deposit (after Ref. [52]), showing the occurrence of type-II orebodies.

2.2. Ore Types and Mineral Paragenetic Sequence

2.2.1. Ores of Type-I Orebodies

The ore structure of the type-I orebodies is characterized as massive and disseminated with veins in different locations. Ore minerals include cassiterite, arsenopyrite, pyrrhotite, chalcopyrite, sphalerite, galena, lillianite, native bismuth, and bismuthinite. Based on the major mineral (cassiterite, sphalerite, and galena) contents, the ores of the type-I orebodies can be divided into Sn, Sn–Pb–Zn, and Pb–Zn ores (Figure 4). According to mineral assemblages and textural relationships, the type-I orebodies experienced four stages of mineralization (stage 1 to stage 4) (Figure 5). Stage 1 is the oxide mineral stage, in which wolframite, scheelite, and a small amount of cassiterite form. Stage 2 is the cassiterite–sulfide stage, in which cassiterite, arsenopyrite, pyrite, and pyrrhotite form as well as gangue minerals including quartz, fluorite, and chalorite. Stage 3 is the Cu–Pb–Zn sulfide stage, in which chalcopyrite, sphalerite, and galena form as well as trace amounts of stannite, bismuthinite,

native bismuth, and lillianite (Figure 6). Stage 4 is the calcite stage, in which quartz, calcite and trace amounts of galena form.

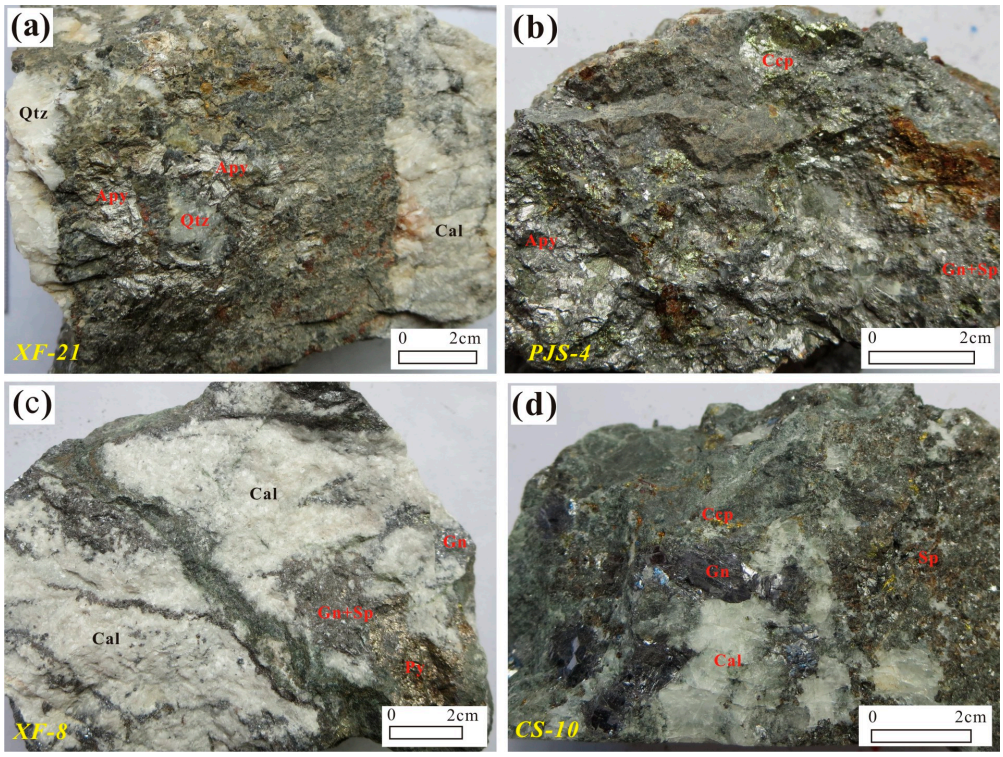

Figure 4. Photographs of typical ore specimens of the type-I orebodies: (**a**) arsenopyrite-rich Sn ore in Xinfeng; (**b**) arsenopyrite-rich Sn–Pb–Zn ore in Paojinshan; (**c**) marble-hosted Pb–Zn ore in Xinfeng, and (**d**) chalcopyrite-bearing Pb–Zn ore in Chashan. Mineral abbreviation: Qtz = quartz, Cal = calcite, Apy = Arsenopyrite, Ccp = chalcopyrite, Sp = sphalerite, Gn = galena, and Py = pyrite.

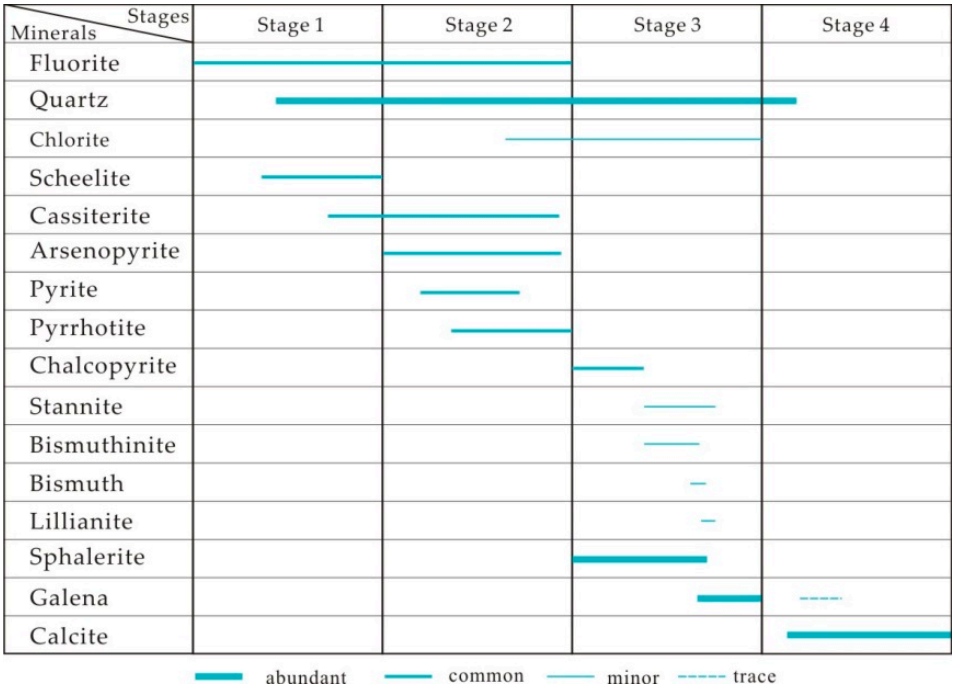

Figure 5. Paragenetic sequences of the minerals in the type-I orebodies.

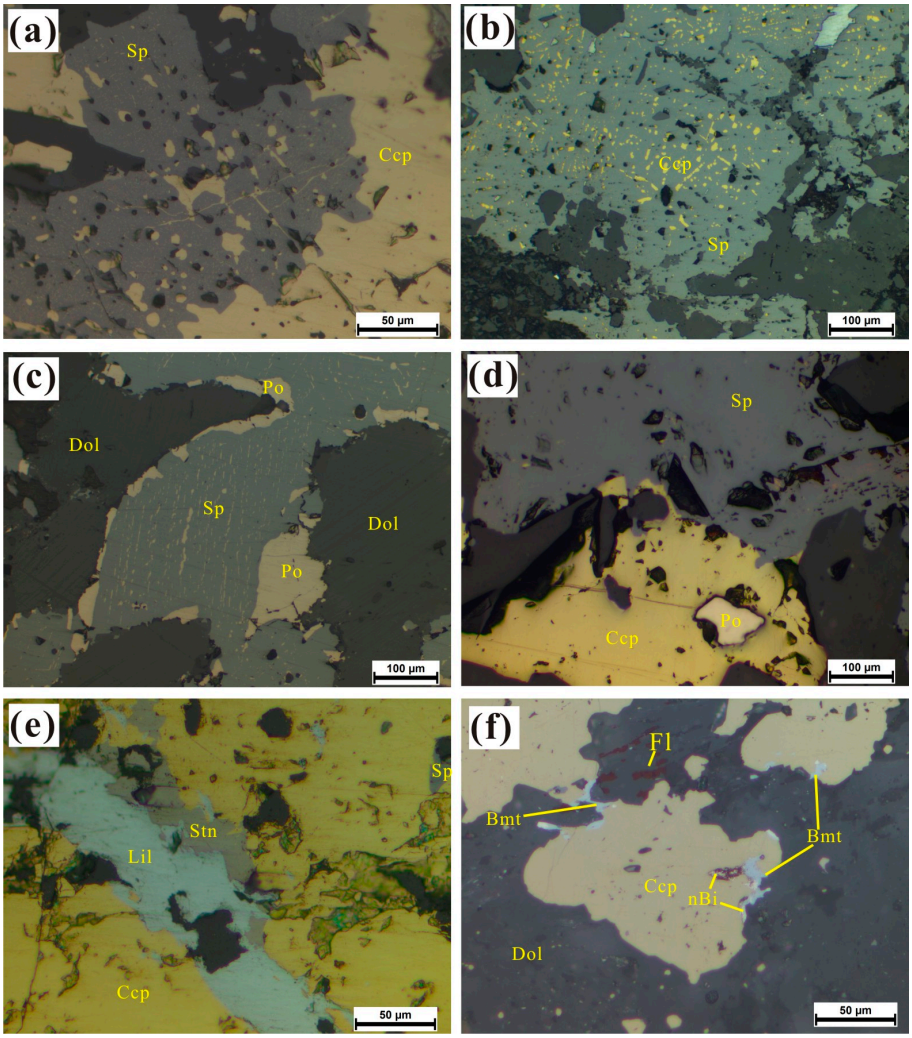

Figure 6. Photomicrographs of ores in the type-I orebodies: (**a**) fine chalcopyrite (Ccp) inclusions in sphalerite (Sp) in Sn ores in Xinfeng; (**b**) vein and drip chalcopyrite inclusions in sphalerite in Paojinshan; (**c**) pyrrhotite (Po) inclusions in sphalerite in Xinfeng; (**d**) inclusion-free sphalerite with chalcopyrite in Chashan; (**e**) lillianite (Lil) and stannite (Stn) replacing in chalcopyrite in Paojinshan, and (**f**) bismuthinite (Bmt) and native bismuth (nBi) surrounding chalcopyrite in Xinfeng.

2.2.2. Ores of Type-II Orebodies

Based on their structure, the ores in the type-II orebodies in the granitic porphyry dikes can be divided into disseminated ores (Figure 7a) and veinlet ores (Figure 7b). The disseminated ores are located in the western dikes, while veinlet ores are located in the eastern dikes. The ore minerals of type-II orebodies include cassiterite, arsenopyrite, pyrite, pyrrhotite (Figure 8a), chalcopyrite, sphalerite (Figure 8b), galena, and boulangerite (Figure 8b,c). Gangue minerals contain quartz, topaz, fluorite, schorl (Figure 8c), and calcite. According to textural relationships between these minerals, the type-II Sn–Pb–Zn orebodies experienced four stages of mineralization (stage 1 to stage 4). Stage 1 is the oxide mineral stage, in which topaz, schorl, flurite, quartz, and trace amounts of scheelite and cassiterite form. Stage 2 is the cassiterite–sulfide stage, in which scassiterite, arsenopyrite, pyrite, and pyrrhotite form as well as gangue minerals including quartz and fluorite. Stage 3 is the Pb–Zn sulfide stage, in which sphalerite, galena and chalcopyrite with trace amounts of tetrahedrite and stannite form. Stage 4 is the boulangerite–calcite stage, in which abundant boulangerite forms. The paragenetic sequences of minerals in the type-II orebodies are summarized in Figure 9.

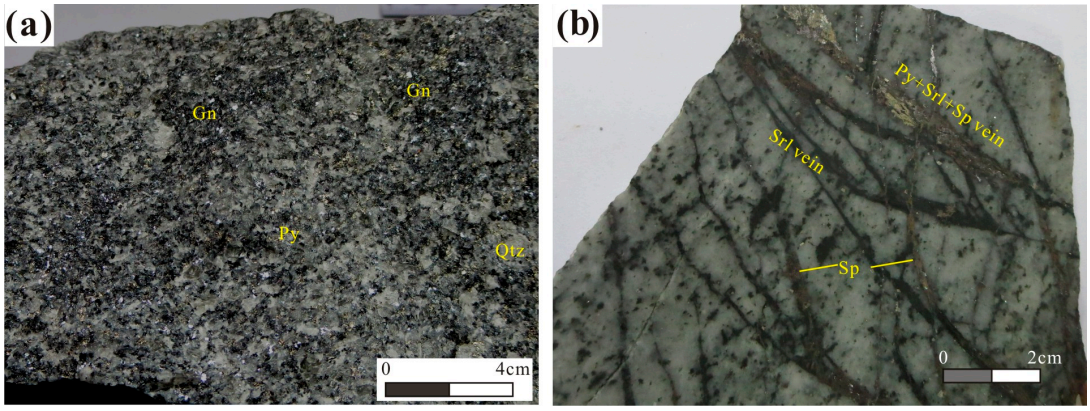

Figure 7. Photographs of typical ore specimens from the type-II orebodies: (**a**) granitic porphyry-hosted disseminated Sn–Pb–Zn ores; and (**b**) granitic porphyry-hosted veinlet Sn–Pb–Zn ores. Srl = schorl; for other abbreviations see Figure 4.

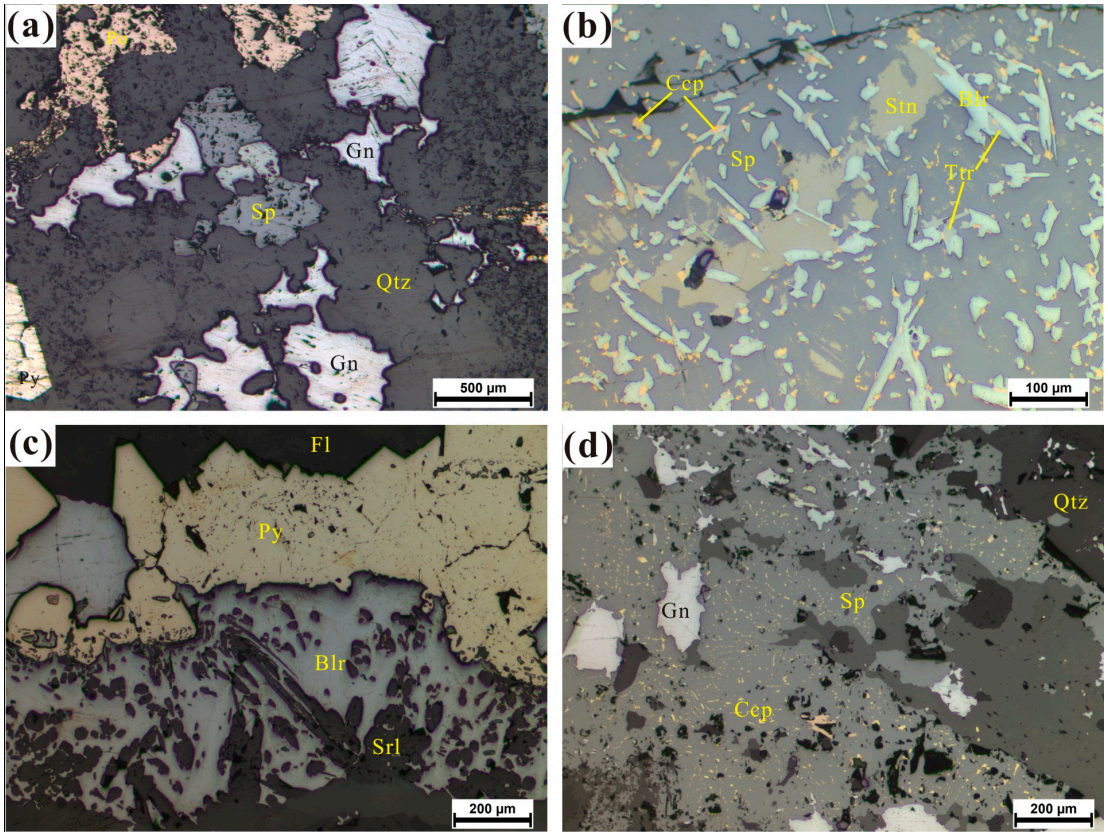

Figure 8. Photomicrographs of ores in the type-II orebodies: (**a**) disseminated ores of the granitic porphyry: pyrrhotite (Po), pyrite (Py), sphalerite (Sp), and galena (Gn) are disseminated and replace the quartz (Qtz); (**b**) veinlet ores containing sphalerite, stannite (Stn), chalcopyrite (Ccp), tetrahedrite (Ttr), and boulangerite (Blr) mineral assemblages; (**c**) veinlet ores composed of schorl (Srl), fluorite (Fl), pyrite, and boulangerite; and (**d**) veinlets composed of sphalerite and galena, showing fine chalcopyrite inclusions in the sphalerite.

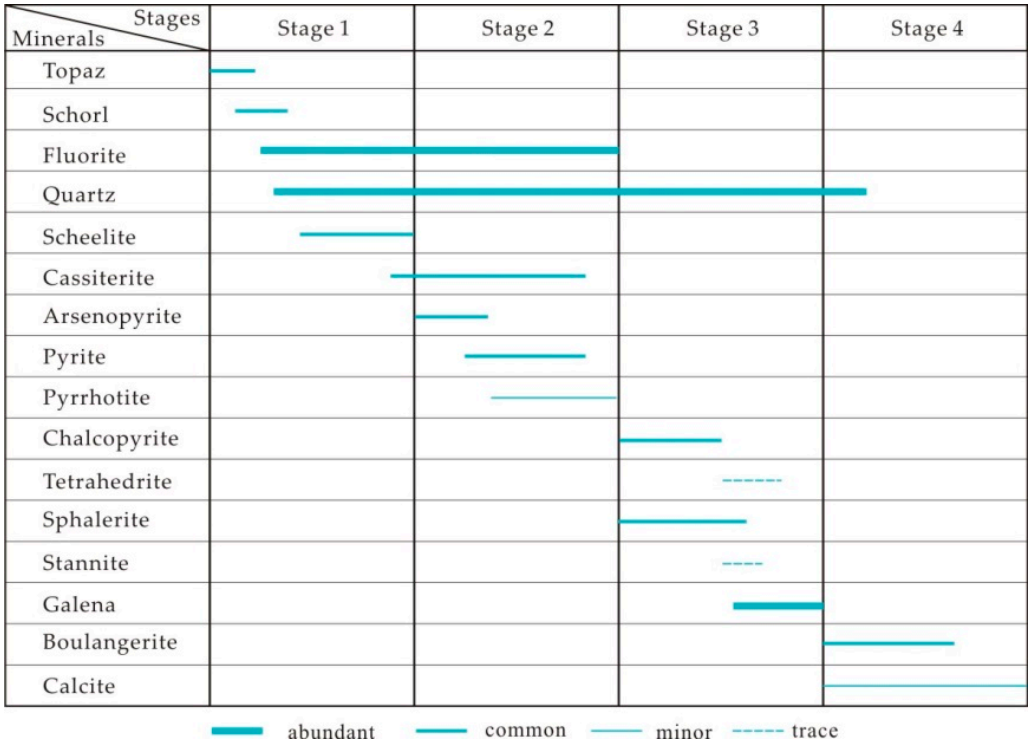

Figure 9. Paragenetic sequences of the minerals of the type-II orebodies.

3. Sampling and Analyses

3.1. Sample Sites

Ore samples were collected from underground workings of the Xinfeng, Tangguanpu, Chashan, and Paojinshan deposits. The locations, types, and ore minerals compositions of samples are listed in Table 1.

Table 1. Location, types, and ore minerals of the analyzed samples from the Xianghualing orefield.

Sample No.		Location	Ore Types	Oxide and Sulfide Minerals	Associated Gangue
Type-I orebodies in Xinfeng deposit					
1	XF3	182 m Level	Disseminated Pb–Zn ores	Sp, Gn, Ccp	Qtz, Chl, Cal, Act
2	XF6	182 m Level	Disseminated Pb–Zn ores	Sp, Gn, Py, Po, Sch	Qtz, Fl, Chl, Cal
3	XF8	182 m Level	Marble hosted veinlet Pb–Zn ores	Sp, Gn, Ccp, Po, Py, Apy, Cst	Cal, Qtz
4	XF12	182 m Level	Marble hosted veinlet Pb–Zn ores	Sp, Gn, Py, Po	Chl, Cal,
5	XF17	182 m Level, Line 15	Marble hosted veinlet Pb–Zn ores	Po, Sp, Apy, Gn	Cal, Chl
6	XF18	182 m Level, Line 17	Marble hosted veinlet Pb–Zn ores	Gn, Sp, Po, Apy	Cal
7	XF19	182 m Level, Line 51	Marble hosted veinlet Pb–Zn ores	Gn, Sp, Po, Apy, Py, Cst	Cal

Table 1. *Cont.*

Sample No.		Location	Ore Types	Oxide and Sulfide Minerals	Associated Gangue
Type-I orebodies in Xinfeng deposit					
8	XF21	182 m Level, Line 59	Disseminated Sn ores	Apy, Ccp, Cst, Sp, Py, Bmt, nBi	Qtz, Cal
9	XF23	182 m Level, Line 59	Disseminated Sn ores	Apy, Py, Ccp, Cst, Sp, Sch, Bmt, nBi	Qtz, Cal
10	XF25	182 m Level, Line 59	Disseminated Sn ores	Po, Apy, Py, Cst, Ccp, Sp, Bmt, nBi	Qtz, Cal
Type-I orebodies in Tangguanpu deposit					
11	TG-1	645 m Level, Line 90	Massive Sn–Pb–Zn ores	Sp, Gn, Apy, Py, Cst, Ccp, Sch	Qtz, Fl
12	TG-2	645 m Level, Line 92	Disseminated Sn–Pb–Zn ores	Sp, Gn, Apy, Py, Cst, Ccp	Qtz, Fl
13	GY-1	75–100 m Level	Disseminated and vein Sn–Pb–Zn ores	Po, Sp, Gn, Py, Apy, Ccp, Stn	Qtz, Fl
14	GY-2	75–100 m Level	Disseminated Sn–Pb–Zn ores	Gn, Py, Ccp, Apy, Cst,	Qtz
15	GY-3	75–100 m Level	Massive Pb–Zn ores	Sp, Gn, Py, Ccp	Qtz, Cal
16	GY-4	75–100 m Level	Disseminated Sn–Pb–Zn ores	Sp, Gn, Ccp, Cst, Apy, Cst, Py	Qtz, Fl, Cal
17	GY-5	75–100 m Level	Disseminated and vein Sn–Pb–Zn ores	Sp, Gn, Apy, Py, Ccp, Cst, Stn, Sch	Qtz, Fl, Cal
Type-I orebodies in Paojinshan deposit					
18	PJS1	237 m Level	Disseminated Sn–Pb–Zn ores	Sp, Ccp, Cst, Py, Po	Cal, Act, Qtz
19	PJS2	237 m Level	Disseminated Sn–Pb–Zn ores	Sp, Gn, Cst, Sch	Qtz, Fl, Cal
20	PJS3	237 m Level	Disseminated Sn–Pb–Zn ores	Mag, Sp, Py, Ccp, Cst	Cal, Qtz, Fl,
21	PJS4	237 m Level	Disseminated Sn–Pb–Zn ores	Apy, Ccp, Py, Sp, Gn, Cst, Sch, Stb, Stn	Qtz, Fl, Cal
22	PJS5	237 m Level	Disseminated Sn–Pb–Zn ores	Sp, Gn, Ccp, Py, Apy, Cst	Qtz, Fl, Cal
23	PJS6	237 m Level	Disseminated sulfides and vein Sn–Pb–Zn ores	Sp, Ccp, Apy, Gn, Po, Cst, Py, nBi, Bmt	Qtz, Act, Fl, Cal
24	PJS20	237 m Level	Massive Sn–Pb–Zn ores	Po, Sp, Gn, Apy, Cst, Ccp	Qtz, Cal
Type-I orebodies in Chashan deposit					
25	CS5	327 m Level	Disseminated Pb–Zn ores	Sp, Gn, Ccp, Po, Sch	Dol, Cal, Fl
26	CS11	330 m Level	Disseminated Pb–Zn ores	Sp, Gn, Apy, Ccp, Py	Dol, Cal, Qtz
27	CS12	330 m Level	Disseminated Pb–Zn ores	Sp, Gn, Apy, Ccp	Dol, Cal, Fl
28	CS13	330 m Level	Disseminated Pb–Zn ores	Sp, Gn, Ccp, Py, Sch	Dol, Cal, Qtz
29	CS17	490 m Level	Disseminated Pb–Zn ores	Sp, Gn, Ccp, Po	Dol, Cal, Fl

Table 1. *Cont.*

Sample No.		Location	Ore Types	Oxide and Sulfide Minerals	Associated Gangue
Type-II orebodies in Tangguanpu deposit					
30	BB1	667 m Level, Line 100	Granitic porphyry hosted disseminated Sn–Pb–Zn ores	Gn, Sp, Po, Cst, Apy	Qtz, Fsp, Fl
31	BB2	667 m Level, Line 100	Granitic porphyry hosted disseminated Sn–Pb–Zn ores	Sp, Gn, Apy, Cst, Py	Qtz, Fsp, Fl
32	BB4	667 m Level, Line 100	Granitic porphyry hosted disseminated Sn–Pb–Zn ores	Sp, Gn, Apy, Cst, Py	Qtz, Fsp, Fl
33	BB5	667 m Level, Line 100	Granitic porphyry hosted disseminated Sn–Pb–Zn ores	Sp, Gn, Apy, Cst, Py	Qtz, Fsp, Fl
34	TGP6	No.I dike	Granitic porphyry hosted veinlet Sn–Pb–Zn ores	Sp, Py, Apy, Ccp, Cst, Blr, Gn	Qtz, Cal, Fl
35	TGP10	No.I dike	Granitic porphyry hosted veinlet Pb–Zn ores	Sp, Gn, Apy, Blr,	Qtz, Cal, Fl
36	TGP16	No.I dike	Granitic porphyry hosted veinlet Pb–Zn ores	Gn, Apy, Blr	Qtz, Srl, Toz, Fl
37	TGP19	No.I dike	Granitic porphyry hosted veinlet Pb–Zn ores	Sp, Gn, Apy	Qtz, Cal, Fl
38	TGP21	No.I dike	Granitic porphyry hosted veinlet Sn–Pb–Zn ores	Blr, Sp, Py, Apy, Ccp, Stn, Cst	Toz, Qtz, Fl
39	TGP31	No.I dike	Granitic porphyry hosted veinlet Pb–Zn ores	Sp, Gn, Apy, Blr, Ccp	Toz, Qtz, Fl

Abbreviations: Sp = sphalerite, Gn = galena, Ccp = chalcopyrite, Qtz = quartz, Chl = chlorite, Cal = calcite, Act = actinolite, Py = pyrite, Po = pyrrhotite, Sch = scheelite, Fl = fluorite, Apy = Arsenopyrite, Cst = cassiterite, Bmt = bismuthinite, nBi = Bismuth, Fsp = feldspar, Blr = boulangerite, Srl = schorl, Toz = topaz, Stn = stannite, Dol = dolomite.

3.2. Whole-Rock Geochemical Analyses

A total of 39 representative ores samples from the Xianghualing orefield were analyzed at Australia Laboratory Services (ALS), ALS Chemex in Guangzhou, China. Bulk samples were processed using perchloric, nitric, hydrofluoric, and hydrochloric acids (four acids), digested, and then the In contents were measured using inductively-coupled plasma-mass spectrometry, with detection limits of 0.005 to 500 ppm. Other elements, including S, Ti, Mn, Fe, Co, Ni, Cu, Zn, As, Mo, Ag, Cd, Sn, Sb, W, Pb, and Bi, were processed with four acids and sodium peroxide flux and were analyzed using inductively-coupled plasma-atomic emission spectroscopy.

3.3. Electron-Probe Microanalyses

Minerals were identified in polished thick sections using standard reflected-light microscopy techniques. The results of the bulk-rock geochemistry were used to select In-rich samples for detailed mineralogical and in situ compositional studies. Electron-probe microanalyses (EPMA) with backscattered electron images observation and X-ray elemental mapping were conducted using a Shimadzu EPMA-1720H electron microprobe at the School of Geosciences and Info-physics, Central South University, Changsha, China. The operating conditions of the electron microprobe were as follows: 15-kV accelerating voltage, 60-nA beam current, and 1-μm diameter electron beam. The X-ray lines used to analyze the different elements were as follows: S ($K\alpha$), Mn ($K\alpha$), Fe ($K\alpha$), Cu ($K\alpha$), Zn ($K\alpha$), Ga ($L\alpha$), Cd ($L\alpha$), In ($L\alpha$), and Sn ($L\alpha$). Mineral and metal standards used for elemental calibrations included chalcopyrite (S, Fe, and Cu), metallic manganese (Mn), sphalerite (Zn), gallium arsenide (Ga), greenockite (Cd), indium antimonide (In), and herzenbergite (Sn). The resulting data was corrected by the atomic number (Z), absorption (A) and fluorescence (F) effects (ZAF)- method using proprietary Shimadzu software. The minimum detection limit of Cu and In was 0.02 wt %, that of Zn, Fe, Cd, and Ga was 0.03 wt %, that of Mn was 0.04 wt %, and that of Sn was 0.07 wt %.

Because the In-Lα (λ = 3.772Å) line experienced interference from the Sn-Lη line (λ = 3.789 Å) [13,53,54], and the Ga-Lα (λ = 11.292 Å) line experienced interference from the In-Lα (λ = 11.316 Å) line [13], 22 ppm In per 1 wt % Sn in stannite, and 500 ppm Ga per 1 wt % In in sphalerite were added to correct for this interference (as per the practice of Ref. [13]).

4. Results

4.1. Chemical Composition of Ores

Twenty-nine samples of Sn ores, Sn–Pb–Zn ores, and Pb–Zn ores from the type-I orebodies and ten samples of disseminated ores and veinlet ores from the type-II orebodies were analyzed for In and related elements. The results are listed in Table 2.

4.1.1. Type-I Orebodies

In the Xinfeng deposit, the Pb–Zn ores from the type-I orebodies contain 1.48–10.75 wt % Pb, 1.40–17.05 wt % Zn, <0.01–0.26 wt % Sn, and 10–180 ppm In with 1000In/Zn = 0.52–1.98; and the Sn ores contain 1.75–4.17 wt % Sn, low Pb and Zn, 0.52–1.72wt % Cu, and 170–410 ppm In with 1000In/Zn = 136.67–366.67, which is the highest In/Zn ratio in the deposit.

Sn–Pb–Zn ores from the Tangguanpu deposit contain 0.07–3.34 wt % Sn (avg. 1.42 wt %), 2.83–26.10 wt % Pb, 0.04–16.75 wt % Zn, 0.11–0.96 wt % Cu, and 10–1680 ppm In with 1000In/Zn = 0.35–25.

Sn–Pb–Zn ores from the Paojinshan deposit contain 0.02–1.19 wt % Sn (avg. 0.46 wt %), 0.43–23.7 wt % Zn (avg. 10.98 wt %), 0.02–7.98 wt % Pb, 0.01–6.15 wt % Cu, and 11.55–620 ppm In with 1000In/Zn = 0.32–16.42 wt %.

Pb–Zn ores from the Chashan deposit contain 4.30–26.50 wt % Zn, 3.12–26.20 wt % Pb, 0.05–0.50 wt % Cu, and 0.79–550 ppm In.

Thus, due to their different occurrences and mineral assemblages, the ores from the type-I orebodies contain variable In contents of 0.79–1680 ppm and 1000In/Zn ratio of 0.32–366.67.

Table 2. Analytical results of selected ores from the Xianghualing orefield.

Units / Detection Limits	1000In/Zn	In ppm 0.005	Sn wt % 0.01	Cd ppm 0.5	Zn wt % 0.01	Pb wt % 0.01	Cu ppm 1	Fe wt % 0.1	Mn ppm 5	Ni ppm 1	Co ppm 1	W ppm 10.00	Bi ppm 2	As wt % 0.01	Sb ppm 5	Ag ppm 0.5	Mo ppm 1	Ti wt % 0.01	S wt % 0.1
Type-I orebodies in Xinfeng deposit																			
XF3	0.88	150.00	<0.01	>1000	17.05	10.75	352	9.5	6730	<1	33	70	1090	0.06	<5	>100	<1	<0.01	12.0
XF6	0.52	50.00	<0.01	630.0	9.53	2.92	181	6.7	3960	<1	9	1810	178	<0.01	<5	89.3	<1	<0.01	6.4
XF8	0.64	50.00	0.26	704.0	7.77	6.20	3450	9.5	14,450	1	<1	70	23	5.55	395	>100	2	<0.01	9.4
XF12	1.21	180.00	0.02	>1000	14.85	5.59	183	7.3	12,600	<1	<1	10	<2	0.07	132	>100	<1	0.01	11.9
XF17	1.17	50.00	0.01	470.0	4.26	1.48	283	10.1	5680	1	3	20	2	0.16	256	83.9	<1	<0.01	8.4
XF18	0.71	10.00	0.05	157.5	1.40	3.04	71	2.2	5920	1	<1	<10	<2	0.21	355	>100	<1	0.01	2.1
XF19	1.98	50.00	0.09	288.0	2.52	4.11	121	8.6	10,800	1	5	30	<2	3.12	395	69.1	<1	<0.01	8.3
XF21	366.67	220.00	1.75	7.1	0.06	0.02	5220	11.4	396	<1	1	110	339	4.75	306	14.3	1	<0.01	7.4
XF23	283.33	170.00	1.89	6.3	0.06	0.01	9810	30.0	279	<1	3	1150	409	7.81	72	21.2	6	<0.01	18.5
XF25	136.67	410.00	4.17	26.1	0.30	0.11	17,200	29.8	675	<1	1	60	877	>10.0	53	81.4	9	<0.01	19.8
Mean (n = 10)	79.38	134.00	0.83	429.9	5.78	3.42	3687	12.5	6149	1	6	370	334	3.17	197	75.9	2	0.01	10.4
Type-I orebodies in Tangguanpu deposit																			
TG-1	14.67	1680.00	1.76	>1000	11.45	11.90	3580	11.9	748	3	1	1000	10	6.00	1175	>100	2	0.01	17.1
TG-2	7.35	620.00	1.35	853.0	8.43	13.45	1730.	8.5	84	5	9	50	17	6.62	2680	>100	2	<0.01	12.7
GY-1	0.35	10.00	0.66	603.0	2.82	2.83	1070	10.7	406	12	4	10	<2	<0.01	5380	88.6	1	0.22	7.9
GY-2	5.00	10.00	0.71	38.8	0.20	14.55	2770	12.0	183	2	14	20	124	>10.0	904	>100	2	<0.01	9.4
GY-3	1.61	270.00	0.07	>1000	16.75	12.10	2020	11.1	961	1	1	60	731	7.23	299	>100	1	<0.01	16.2
GY-4	25.00	10.00	2.05	30.5	0.04	26.10	7560	18.1	5650	54	5	20	310	1.74	299	>100	11	0.07	6.7
GY-5	20.00	30.00	3.34	55.3	0.15	24.40	9620	8.4	6020	22	9	6170	291	3.37	406	>100	5	0.02	9.0
Mean (n = 7)	10.57	375.71	1.42	511.5	5.69	15.05	4050	11.5	2007	14	6	1047	212	5.00	1592	98.4	3	0.05	11.3
Type-I orebodies in Paojinshan deposit																			
PJS1	0.42	80.00	0.72	>1000	18.90	0.02	4080	12.3	2950	4	<1	110	197	0.88	29	23.1	<1	0.02	12.0
PJS2	0.49	70.00	1.19	>1000	14.15	7.98	143	9.2	2390	9	26	1010	874	0.26	<5	>100	10	0.02	9.7
PJS3	2.55	110.00	0.29	397.0	4.32	0.03	299	23.7	4510	4	1	20	80	0.02	<5	3.0	<1	0.04	3.3
PJS4	16.42	70.60	0.58	33.6	0.43	0.96	61,500	29.9	200	13	31	1420	1830	>10.0	809	>100	5	0.01	21.7
PJS5	0.34	40.00	0.02	883.0	11.75	7.37	3110	7.7	1420	8	<1	20	9	6.34	729	>100	2	0.09	11.1
PJS6	2.62	620.00	0.03	>1000	23.70	2.61	52,400	14.8	1250	19	11	50	1075	1.86	74	>100	4	0.03	22.7
PJS20	0.32	11.55	0.39	245.0	3.63	2.23	357	14.9	1100	5	2	17	4	0.13	79	63.9	<1	0.10	7.9
Mean (n = 7)	3.31	143.16	0.46	651.2	10.98	3.03	17412	16.1	1974	9	10	378	581	1.58	247	70.0	3	0.04	12.6
Type-I orebodies in Chashan deposit																			
CS5	0.02	0.79	<0.01	236.0	4.30	3.12	2990	2.8	4100	3	2	368	5	0.02	17	11.3	7	0.05	3.5
CS11	4.63	406.00	0.02	567.0	8.76	12.20	1120	17.2	8500	<1	<1	<10	124	0.75	164	>100	<1	<0.01	16.8
CS12	2.77	550.00	0.01	>1000	19.85	6.29	968	25.5	17,400	2	<1	<10	260	>10.0	702	>100	1	<0.01	26.2
CS13	0.03	9.06	0.01	>1000	26.50	17.20	4960	2.8	1100	1	4	1010	6	0.01	65	55.5	2	0.02	17.4
CS17	1.50	347.00	<0.01	>1000	23.10	26.20	486	17.1	5800	<1	<1	20	<2	0.43	548	>100	<1	<0.01	26.0
Mean (n = 5)	1.79	262.57	0.01	760.6	16.50	13.00	2104	13.1	7380	2	2	284	79	2.2	299	73.3	2	0.02	18.0
Type-I mean (n = 29)	31.03	216.72	0.74	559.7	8.86	7.79	6815	13.2	4354	6	6	508	306	3.10	564	79.5	3	0.03	12.5
Type-II orebodies in Tangguanpu deposit																			
BB1	1.70	80.00	0.11	437.0	4.70	10.00	475	6.3	190	1	1	50	25	0.64	685	>100	2	<0.01	7.6
BB2	3.16	60.00	1.37	195.5	1.90	0.01	281	5.4	118	1	3	120	43	0.67	69	9.9	3	<0.01	4.1
BB4	3.40	70.00	1.44	233.0	2.06	0.02	245	4.5	124	1	1	10	26	0.24	19	9.8	3	<0.01	3.6
BB5	2.80	40.00	0.59	155.5	1.43	0.03	307	6.8	265	1	2	50	49	1.30	117	10.8	3	<0.01	4.4
TGP6	1.29	56.20	0.35	397.0	4.36	1.40	295	3.8	600	9	30	13	3	0.51	1420	86.2	6	0.02	3.9
TGP10	0.71	24.80	0.01	318.0	3.49	1.76	519	11.1	1200	11	115	23	12	3.46	496	94.1	11	0.02	10.1
TGP16	25.00	10.00	<0.01	4.7	0.04	6.31	22	1.2	100	20	6	<10	20	0.63	474	>100	3	0.02	1.5
TGP19	1.22	83.40	0.16	524.0	6.82	10.25	929	6.6	600	11	10	40	<2	0.67	25400	>100	1	0.29	8.5
TGP21	2.58	152.00	0.29	481.0	5.89	13.65	2330	6.8	600	10	3	880	<2	1.51	60800	>100	1	0.31	11.5
TGP31	2.15	65.70	<0.01	281.0	3.05	2.77	339	2.4	200	3	19	<10	<2	0.30	2090	>100	2	0.05	3.6
Mean (n = 10)	4.40	64.21	0.43	302.7	3.37	4.62	574	5.5	400	7	19	121	18	0.99	9157	71.1	4	0.08	5.9

4.1.2. Type-II Orebodies

Ores from the type-II orebodies contain <0.01–1.44 wt % Sn, 0.01–13.65 wt % Pb, 0.04–6.82 wt % Zn, and 10–152 ppm In with 1000In/Zn = 0.71–25.00.

4.1.3. Correlations among Significant Elements

In the In–Sn, In–Cu, and In–Zn binary diagrams (Figure 10a–c), the In/Sn, In/Cu, and In/Zn ratios of the type-II orebodies are characterized by a narrower range than that of the type-I orebodies. In addition, Cd and Zn are positively correlated with Cd/Zn from 0.005 to 0.05 (Figure 10d).

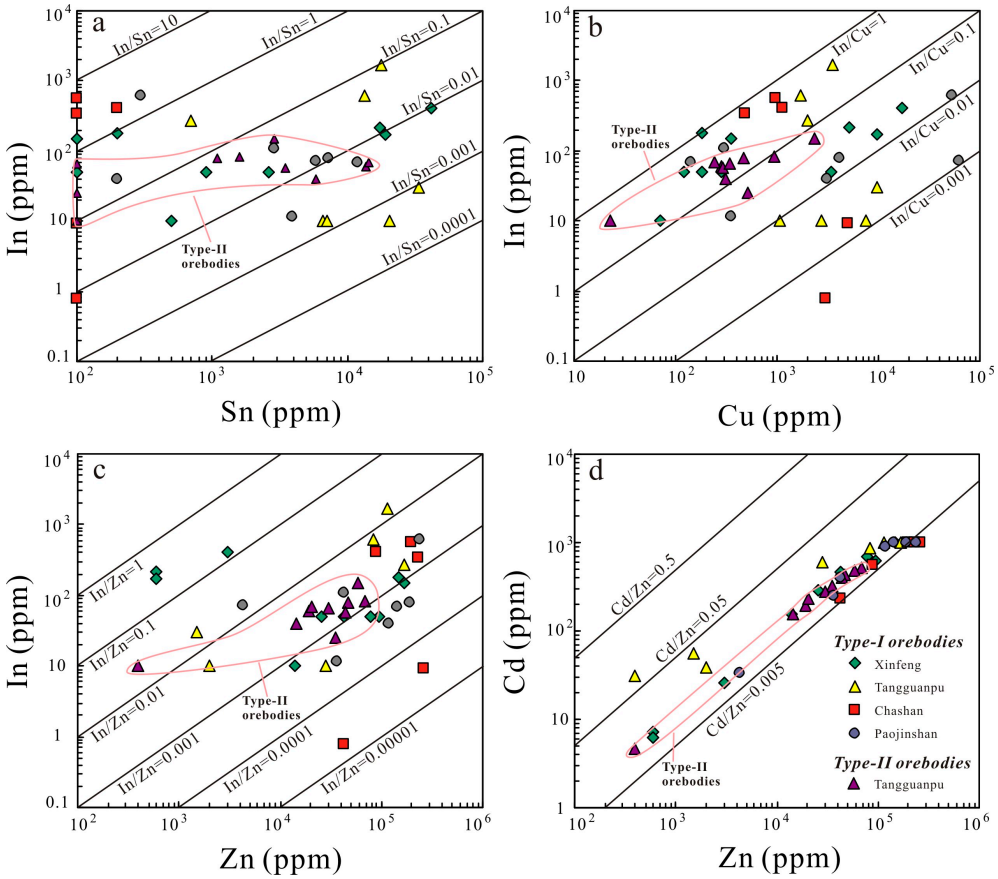

Figure 10. Binary diagrams of (**a**) In–Sn, (**b**) In–Cu, (**c**) In–Zn, and (**d**) Zn–Cd for ores, showing the variation of the two types of orebodies.

4.2. Chemistry of Ore Minerals

Sphalerite, chalcopyrite and stannite were analyzed for both types of orebodies.

4.2.1. Sphalerite

A total of 100 spots of sphalerite were analyzed for the two types of orebodies in the orefield. The results are listed in Table 3. The In contents of the sphalerite in the type-I orebodies varies from <0.02 to 21.96 wt %. The sphalerite from the Sn ores in the Xinfeng deposit (i.e., sample No. x21d1–x25d4) contains high In (0.98–21.96 wt %). The sphalerite from the Sn–Pb–Zn ores in the Tangguanpu deposit contains 0.26–0.35 wt % In, and while that from the Paojinshan deposit contains 0.06–0.70 wt % In. The sphalerite from the Pb–Zn ores contains low In, e.g., <0.02–0.18 wt % (mostly below 0.09 wt %) in Xinfeng (i.e., sample No. x3a1–x17b5) and below the detection limits in Chashan.

Table 3. Electron-probe microanalyses (EPMA) data of sphalerite of the Xianghualing orefield (wt %)

Spots	Zn	Fe	Cu	Sn	In	Cd	Mn	Ga	S	Total
Sphalerite in type-I orebodies of Xinfeng deposit										
x3a1	56.19	8.77	-	-	-	0.43	0.31	-	33.37	99.07
x3a2	58.18	6.81	0.05	-	0.07	0.50	0.25	0.05	33.17	99.08
x3a3	54.89	9.56	0.08	-	0.18	0.50	0.34	0.08	33.33	98.96
x3a4	58.13	7.23	-	-	0.02	0.43	0.25	0.05	33.06	99.17
x3b1	52.94	10.99	0.08	-	0.06	0.47	0.33	0.04	33.30	98.21
x3b2	57.53	6.92	0.04	-	0.03	0.45	0.23	0.07	33.09	98.36
x17a1	54.58	10.07	0.05	-	0.08	0.73	0.37	0.06	33.37	99.31
x17a2	54.36	10.43	0.06	-	0.07	0.71	0.16	0.08	33.27	99.14
x17a3	53.91	10.12	0.06	-	0.07	0.71	0.32	0.07	33.28	98.54
x17a4	55.10	9.77	0.06	-	0.05	0.68	0.28	0.07	33.67	99.68
x17a5	55.58	9.61	0.04	-	0.07	0.74	0.18	0.05	33.29	99.56
x17a6	56.02	9.40	0.11	-	0.07	0.70	0.13	0.06	33.28	99.77
x17b2	54.11	9.98	0.10	-	0.07	0.72	0.26	0.04	33.19	98.47
x17b3	53.04	10.28	1.22	-	0.09	0.69	0.20	0.08	33.28	98.88
x17b4	55.30	9.55	0.09	-	0.07	0.66	0.25	0.07	33.34	99.33
x17b5	55.09	9.63	0.07	-	0.08	0.69	0.08	0.07	33.17	98.88
x21d1	44.96	6.23	6.91	-	6.89	0.45	-	-	32.41	97.85
x21d2	42.75	7.62	8.41	-	6.64	0.36	-	-	32.57	98.35
x21d3	45.72	6.35	7.15	-	8.02	0.38	-	-	32.37	99.99
x21d4	46.31	5.89	6.18	-	6.94	0.43	-	-	32.02	97.77
x21d5	38.84	8.52	10.59	-	7.81	0.41	-	-	32.90	99.07
x21d1a	24.23	7.56	13.57	-	21.33	0.35	-	-	30.65	97.69
x21d1b	24.37	6.86	13.62	-	21.96	0.36	-	-	30.31	97.48
x21d2b	45.43	6.56	6.70	-	7.82	0.42	-	-	32.68	99.61
x21d2c	45.88	6.05	6.54	-	7.12	0.35	-	-	32.42	98.36
x21f1	46.51	6.26	6.31	-	6.08	0.40	-	-	32.35	97.91
x21f2	43.70	7.95	8.33	-	5.57	0.35	-	-	32.66	98.56
x21f3	49.15	4.68	4.85	-	6.64	0.44	-	-	32.11	97.87
x25a1	52.60	9.52	1.52	-	2.15	0.39	-	-	33.17	99.35
x25a2	52.12	9.60	1.56	-	2.40	0.39	-	0.04	32.96	99.07
x25a3	52.03	9.72	1.34	-	2.00	0.42	-	0.05	33.13	98.69
x25b1	50.55	9.71	2.60	-	3.13	0.35	-	-	33.57	99.91
x25b2	52.87	10.05	1.26	-	1.90	0.40	-	0.04	33.34	99.86
x25b3	43.02	11.45	6.84	-	3.14	0.36	-	-	33.21	98.02
x25c1	52.46	9.95	1.85	-	2.12	0.40	-	0.04	33.49	100.31
x25c2	52.95	9.69	1.36	-	2.05	0.44	-	-	33.50	99.99
x25c3	52.68	9.34	1.48	-	2.16	0.43	-	0.03	33.19	99.31
x25d1	55.03	9.18	0.85	-	1.08	0.43	-	-	33.68	100.25
x25d2	54.43	9.02	0.97	-	1.16	0.43	-	0.05	33.46	99.52
x25d3	50.24	10.57	3.28	-	0.96	0.41	-	0.06	33.54	99.06
x25d4	54.85	9.23	0.86	-	0.98	0.40	-	0.04	33.49	99.85
Mean (41)	50.21	8.70	3.26	-	3.48	0.48	0.25	0.05	32.97	98.98
Sphalerite in type-I orebodies of Tangguangpu deposit										
tg1a1	54.38	10.05	0.23	-	0.33	0.63	0.14	-	33.95	99.71
tg1a2	48.35	12.85	4.43	-	0.26	0.53	0.13	-	33.87	100.42
tg1c1	54.96	10.47	0.30	-	0.29	0.64	0.17	-	33.62	100.45
tg1c2	55.47	9.27	0.33	-	0.33	0.70	0.18	-	33.69	99.97
tg1c3	54.51	9.00	0.24	-	0.31	0.67	0.17	0.08	33.34	98.32
tg1c4	54.77	9.32	0.28	-	0.35	0.66	0.16	0.06	33.36	98.96
tg1e1	56.85	8.13	0.29	-	0.32	0.74	0.20	-	33.25	99.78
tg1e2	55.03	9.04	0.31	-	0.31	0.72	0.16	0.04	33.50	99.11
tg1e3	56.62	7.86	0.22	-	0.27	0.82	0.14	0.07	33.59	99.59
Mean (9)	54.55	9.55	0.74	-	0.31	0.68	0.16	0.06	33.57	99.59
Sphalerite in type-I orebodies of Paojingshan deposit										
p4b1.2	54.68	8.04	2.11	-	0.43	0.32	0.07	0.08	33.10	98.83
p4b1.3	53.53	7.25	3.35	-	0.50	0.29	0.04	0.06	33.14	98.16
p4b1.4	55.96	6.66	2.37	-	0.49	0.29	0.04	0.06	33.33	99.20
p4b1.10	57.28	5.64	1.36	-	0.70	0.38	-	0.08	33.01	98.45
p4c1.1	53.59	7.85	2.67	-	0.47	0.35	-	0.11	33.33	98.37
p4c1.3	54.48	8.60	2.47	-	0.38	0.34	0.05	0.05	32.93	99.30
p4c1.4	56.38	7.24	1.69	-	0.41	0.33	0.04	0.07	32.78	98.94
p4c1.5	51.12	9.05	4.61	-	0.37	0.27	-	0.05	33.29	98.76
p4c1.6	54.71	7.88	2.47	-	0.49	0.30	0.08	0.07	33.66	99.66
p4c1.11	56.27	7.51	1.72	-	0.38	0.34	0.04	0.07	33.16	99.49

Table 3. *Cont.*

Spots	Zn	Fe	Cu	Sn	In	Cd	Mn	Ga	S	Total
Sphalerite in type-I orebodies of Paojingshan deposit										
p6a1	59.35	6.24	0.33	-	0.15	0.47	0.19	0.08	33.36	100.17
p6a2	60.60	4.79	0.37	-	0.16	0.46	0.16	0.06	33.39	99.99
p6c1	56.18	9.47	0.07	-	0.06	0.45	0.23	0.05	33.66	100.17
p6c2	55.34	9.76	0.10	-	0.07	0.46	0.24	0.05	33.46	99.48
p6c3	57.53	4.53	2.95	-	0.09	0.43	0.10	0.08	33.21	98.92
p6d1	58.44	6.69	0.33	-	0.10	0.46	0.21	0.07	33.20	99.50
p6d2	58.68	6.30	0.30	-	0.08	0.44	0.19	0.08	33.10	99.17
p6d3	60.45	4.60	0.32	-	0.09	0.45	0.14	0.10	32.85	99.00
p6e1	56.45	4.19	3.70	-	0.90	0.54	-	0.06	32.97	98.81
Mean (19)	56.37	6.96	1.75	-	0.33	0.39	0.12	0.07	33.21	99.17
Sphalerite in type-I orebodies of Chashan deposit										
c3a1	62.45	3.31	0.02	-	-	0.38	0.16	-	33.61	99.93
c3a3	63.06	2.86	0.04	-	-	0.39	0.12	-	33.40	99.87
c3a5	63.13	2.82	-	-	-	0.41	0.11	-	32.69	99.16
c3b4'	60.06	4.23	-	-	-	0.34	0.26	-	33.38	98.27
c3b5'	60.61	4.79	0.02	-	-	0.32	0.34	-	32.01	98.09
c9sa1	58.15	6.98	0.35	-	-	0.22	0.35	-	32.80	98.85
c9sa2	57.39	6.96	0.80	-	-	0.22	0.28	-	32.77	98.42
c9sb1	59.25	6.33	0.03	-	-	0.24	0.35	-	33.05	99.25
c14a1	62.60	3.53	0.02	-	-	0.32	0.24	-	32.96	99.67
c14a2	63.11	2.76	-	-	-	0.31	0.08	-	33.13	99.39
c14c2	62.47	3.36	-	-	-	0.33	0.18	-	33.28	99.62
c14c3	62.18	3.06	0.12	0.11	-	0.34	0.10	-	33.21	99.12
Mean (12)	61.21	4.25	0.18	0.11	-	0.32	0.21	-	33.02	99.30
Sphalerite in type-II orebodies of Tangguangpu deposit										
bb1a1	52.28	13.00	0.21	-	0.11	0.51	0.18	0.06	34.38	100.73
bb1a3	52.55	11.26	0.08	-	0.10	0.55	0.07	0.05	33.86	98.52
bb1a4'	51.66	12.80	0.07	-	0.10	0.52	0.16	0.08	33.44	98.83
bb2a1	52.50	12.26	0.18	-	0.19	0.56	0.13	-	33.65	99.47
bb2a2	52.26	12.66	0.16	-	0.20	0.59	0.12	0.05	33.59	99.63
bb2a3	52.39	12.59	0.14	-	0.20	0.58	0.14	0.07	33.66	99.77
bb2b1	53.40	10.68	0.20	-	0.19	0.61	0.04	0.06	33.67	98.85
bb2b2	53.85	10.20	0.14	-	0.22	0.61	0.04	0.04	33.35	98.45
bb2b3	54.14	10.06	0.15	-	0.19	0.62	0.04	0.05	33.64	98.89
t21a1	54.00	9.56	0.71	0.53	0.21	0.46	0.17	0.08	33.39	99.11
t21a2	43.02	9.70	6.34	5.73	0.29	0.34	0.14	0.06	32.46	98.08
t21a3	53.50	9.18	1.46	0.90	0.19	0.47	0.18	0.05	32.94	98.87
t21a4	56.06	8.40	0.18	-	0.15	0.49	0.20	0.07	33.01	98.56
t21a7	53.57	10.00	0.55	0.30	0.23	0.44	0.16	0.06	32.90	98.21
t21b1	55.62	8.71	0.14	-	0.12	0.48	0.19	0.04	33.09	98.39
t21b2	55.92	8.40	0.35	0.12	0.23	0.50	0.20	-	33.15	98.87
t21e1	57.39	7.25	0.26	-	0.39	0.48	0.17	0.07	33.10	99.11
t33c1	54.03	10.13	0.50	-	0.02	0.46	0.16	0.05	32.96	98.31
t33c2	54.60	10.36	0.04	-	-	0.48	0.24	-	32.94	98.66
Mean (19)	53.30	10.38	0.62	1.52	0.19	0.51	0.14	0.06	33.33	98.91

"-" below detection limits.

The In contents of the sphalerite from the type-II orebodies ranges from <0.02 to 0.39 wt %, with an average of 0.19 wt %.

In the type-I orebodies, In is highly positively correlated with Ga (Figure 11a). The sphalerite from the type-I orebodies in Xinfeng contains high Cu, and there is a high correlation between In and Cu (Figure 11b). Indium correlates poorly with Fe (Figure 11c) and negatively with Fe + Zn (Figure 11d). Indium is poorly correlated with Cd (Figure 11e). The In-rich sphalerite contains 0.35–0.45 wt % Cd (Figure 11e), exhibiting an "Indium window" in the Cu–In–S phases [55]. In addition, Cu is negatively correlated with (Zn + Fe) in sphalerite (Figure 11f).

In sphalerite from the type-II orebodies, there is a poor correlation between In and Ga, Cu, Fe, Zn and Cd (Figure 11a–d), but there is a strong negative correlation between Cu and Zn (Figure 11f).

Indium-rich sphalerite from the Sn ores in Xinfeng was mapped to produce X-ray element-distribution maps for In, Zn, Cu, and Fe (Figure 12). The sphalerite was found to be enriched in Zn in the core (Figure 12d) and enriched in In (Figure 12c) and Cu in the rim (Figure 12e). In the

interior of the sphalerite Cu and Fe (Figure 12e,d) are inhomogeneously due to the effects of fine chalcopyrite inclusions.

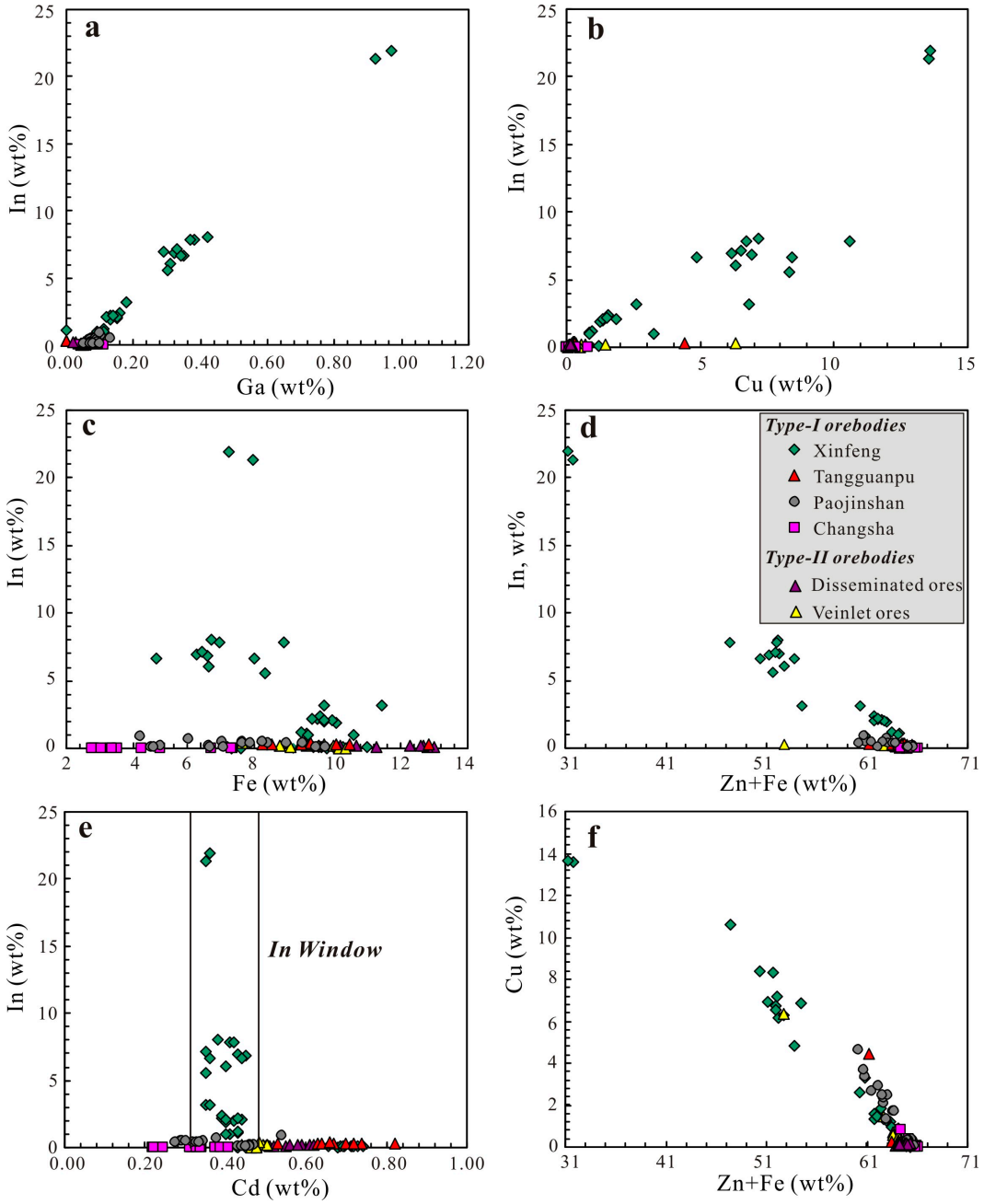

Figure 11. Binary diagrams of (**a**) Ga–In; (**b**) Cu–In; (**c**) Fe–In; (**d**) Zn + Fe–In; (**e**) Cd–In; and (**f**) Zn + Fe–Cu compositions of sphalerite. EPMA data (n = 100), see Table 3.

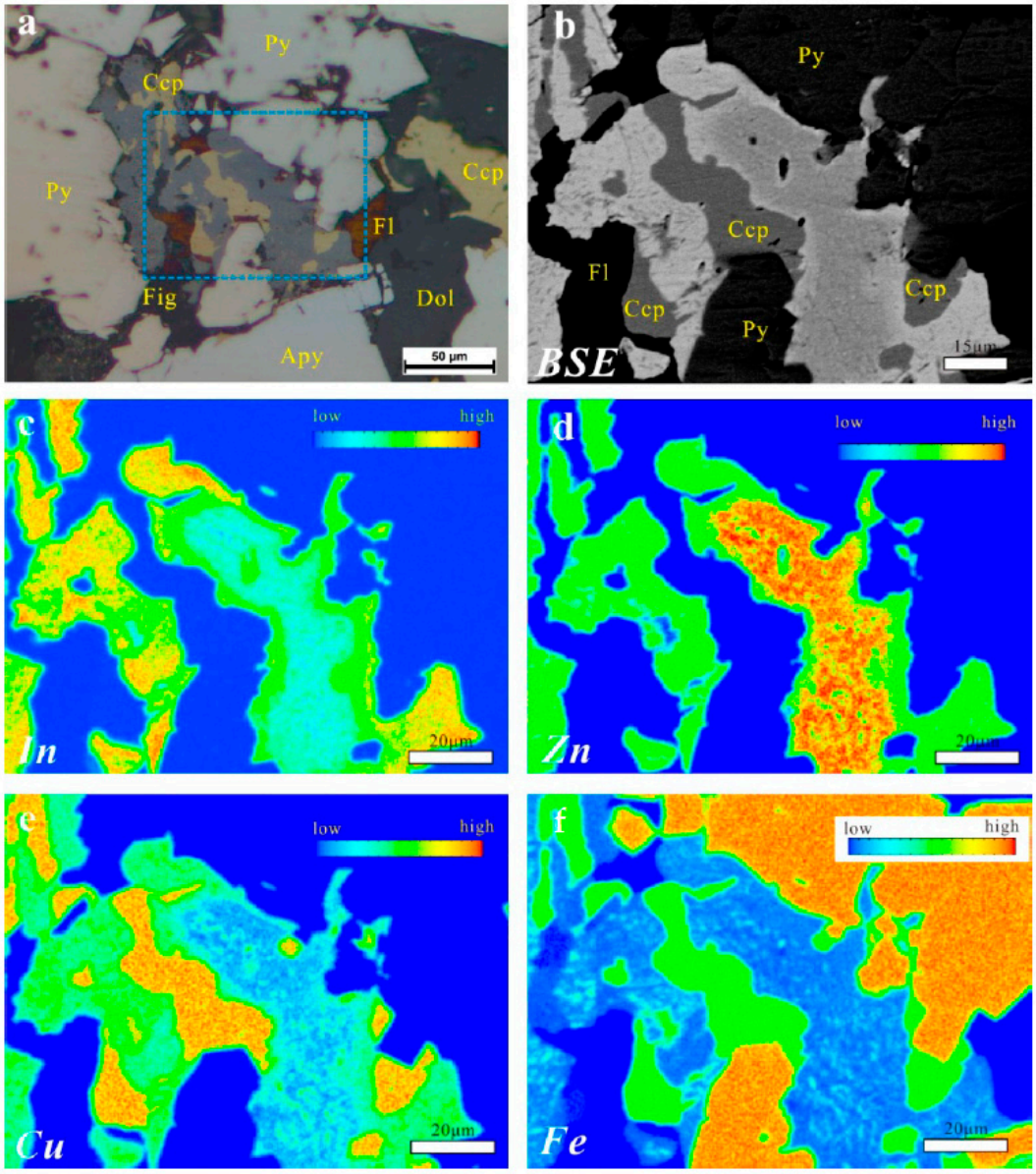

Figure 12. (**a**) Photomicrographs; (**b**) backscattered electron images, and X-ray element-distribution maps for (**c**) In; (**d**) Zn; (**e**) Cu, and (**f**) Fe of high In-bearing sphalerite, showing In and Cu in the rim are richer than in the core, while Zn is richer in the core than in the rim.

4.2.2. Chalcopyrite

Chalcopyrite is common in both types of orebodies, but especially in the type-I orebodies. EPMA data for chalcopyrite from the type-I orebodies in the Xinfeng, Tangguanpu, Chashan and Paojinshan deposits are listed in Table 4. Chalcopyrite from the Xinfeng deposit contains slightly higher In than the chalcopyrite from the other deposits, ranging from 0.04 to 0.40 wt %. The In content of chalcopyrite from the Tangguanpu deposit ranges from <0.02 to 0.07 wt %, form the Paojinshan deposit ranges from 0.02 to 0.10 wt %; and from the Chashan deposit, the value was below the detection limits. In addition, the chalcopyrite contains trace amounts of Zn (<0.03–0.79 wt %). Except for the influence of fine sphalerite inclusions, In and Zn were homogeneous in the chalcopyrite phenocrysts based on the X-ray element-distribution maps for In and Zn (Figure 13).

Table 4. EPMA data of chalcopyrite of the Xianghualing orefield (wt %).

Spots	Zn	Fe	Cu	Sn	In	Cd	Mn	S	Total
Chalcopyrite in type-I orebodies, Xinfeng deposit									
x21a1	-	30.01	34.00	-	0.08	-	-	35.34	99.43
x21a2	0.07	30.05	33.89	-	0.04	-	-	35.23	99.21
x21a3	0.12	30.17	33.83	-	0.10	-	-	35.25	99.35
x21a4	0.06	30.15	34.03	-	0.09	-	-	35.32	99.59
x21a5	0.21	30.36	34.15	-	0.08	-	-	35.58	100.17
x21a6	0.08	30.21	34.07	-	0.09	-	-	35.41	99.78
x21a7	0.07	30.11	33.98	-	0.08	-	-	35.39	99.56
x21f4	0.31	29.58	33.63	-	0.09	-	-	34.96	98.26
x21f5	0.26	29.62	33.78	-	0.09	-	-	35.18	98.67
x21f6	0.18	29.97	33.92	-	0.07	-	-	35.16	99.12
x25a4	0.09	30.23	33.91	-	0.07	-	-	35.15	99.36
x25a5	0.45	29.42	33.80	-	0.07	-	-	34.73	98.02
x25a6	0.17	30.14	34.00	-	0.07	-	-	34.85	99.06
x25a7	0.43	29.43	33.93	-	0.40	-	-	34.93	98.69
x25b4	0.54	30.11	33.74	-	0.06	-	-	35.30	99.21
x25b5	0.06	30.38	33.96	-	0.06	-	-	35.22	99.62
x25b6	0.08	30.29	34.20	-	0.08	-	-	35.32	99.89
x25d5	0.23	30.12	34.16	-	0.06	-	-	35.48	99.82
x25d6	0.05	30.36	34.39	-	0.07	-	-	35.36	100.18
x25d7	0.15	30.01	33.93	-	0.21	-	-	35.28	99.58
x25d8	0.07	29.87	34.03	-	0.10	-	-	34.97	98.97
Mean (n = 21)	0.18	30.03	33.97	-	0.10	-	-	35.20	99.31
Chalcopyrite in type-I orebodies, Tangguangpu deposit									
gy5a1	0.10	30.39	33.98	-	0.03	-	-	35.30	99.72
gy5a2	0.07	30.29	33.71	-	-	-	-	35.13	99.13
gy5a3	0.04	30.55	33.82	-	-	-	-	35.01	99.38
gy2b5	0.10	29.37	33.08	-	0.07	-	-	35.64	98.16
gy2b6	0.09	29.45	33.23	-	0.07	-	-	35.65	98.40
gy2b8	0.05	29.29	33.33	-	0.07	-	-	35.57	98.26
Mean (n = 6)	0.08	29.89	33.53	-	0.04	-	-	35.38	98.84
Chalcopyrite in type-I orebodies, Paojinshan deposit									
p4a1.10	0.09	29.70	33.22	-	0.05	-	-	34.92	97.89
p4a1.11	0.58	29.41	33.19	-	0.05	-	-	35.12	98.35
p4b1.5	0.10	29.39	33.30	-	0.10	-	-	35.12	98.01
p4b1.7	0.16	29.70	33.27	-	0.07	-	-	34.94	98.14
p4b1.8	0.04	29.57	33.44	-	0.09	-	-	34.92	98.06
p4b1.9	0.06	29.69	33.70	-	0.10	-	-	35.30	98.85
p4c1.7	0.11	29.89	33.84	-	0.11	-	-	35.13	99.08
p4c1.8	0.04	29.95	33.68	-	0.08	-	-	35.24	98.99
p4c1.9	0.03	29.93	33.36	-	0.08	-	-	34.95	98.35
p4c1.10	0.07	30.01	33.72	-	0.10	-	-	35.13	99.03
p6a3	0.04	30.11	33.82	0.08	0.05	-	-	35.30	99.40
p6a4	0.16	30.05	33.91	0.08	0.07	-	-	35.01	99.28
p6a5	0.03	30.07	34.01	-	0.07	-	-	35.21	99.39
p6d4	0.09	29.85	33.66	-	0.02	-	-	35.35	98.97
p6d5	0.08	30.02	33.54	-	0.04	-	-	35.75	99.43
p6d6	0.03	30.04	33.43	-	0.02	-	-	35.47	98.99
p6e2	0.08	29.96	34.06	0.07	0.09	-	-	35.12	99.38
p6e3	0.03	30.04	33.77	-	0.05	-	-	35.29	99.18
p6e4	0.03	29.93	33.85	0.07	0.05	-	-	35.23	99.16
Mean (n = 19)	0.10	29.86	33.62	0.08	0.07	-	-	35.18	98.89

Table 4. *Cont.*

Spots	Zn	Fe	Cu	Sn	In	Cd	Mn	S	Total
Chalcopyrite in type-I orebodies, Chashan deposit									
c3-b1	0.06	29.76	33.90	-	-	-	-	35.47	99.19
c3-b2	0.03	29.91	33.90	-	-	-	-	35.94	99.78
c3-b3	0.08	29.44	33.51	-	-	-	-	35.99	99.02
c3-a6	0.10	30.09	34.21	-	-	-	-	35.66	100.06
c3-a7	0.05	30.25	34.13	-	-	-	-	35.49	99.92
c3-a8	0.79	29.71	33.53	-	-	-	-	35.72	99.75
c9sa3	0.10	30.01	33.91	-	-	-	-	34.83	98.85
c9sa4	0.14	30.07	33.81	-	-	-	-	35.08	99.10
c14c1	0.08	30.04	33.81	-	-	-	-	35.28	99.21
c14-c4	0.17	30.25	34.20	-	-	-	-	35.34	99.96
Mean (n = 10)	0.16	29.95	33.89	-	-	-	-	35.48	99.48

"-" below detection limits.

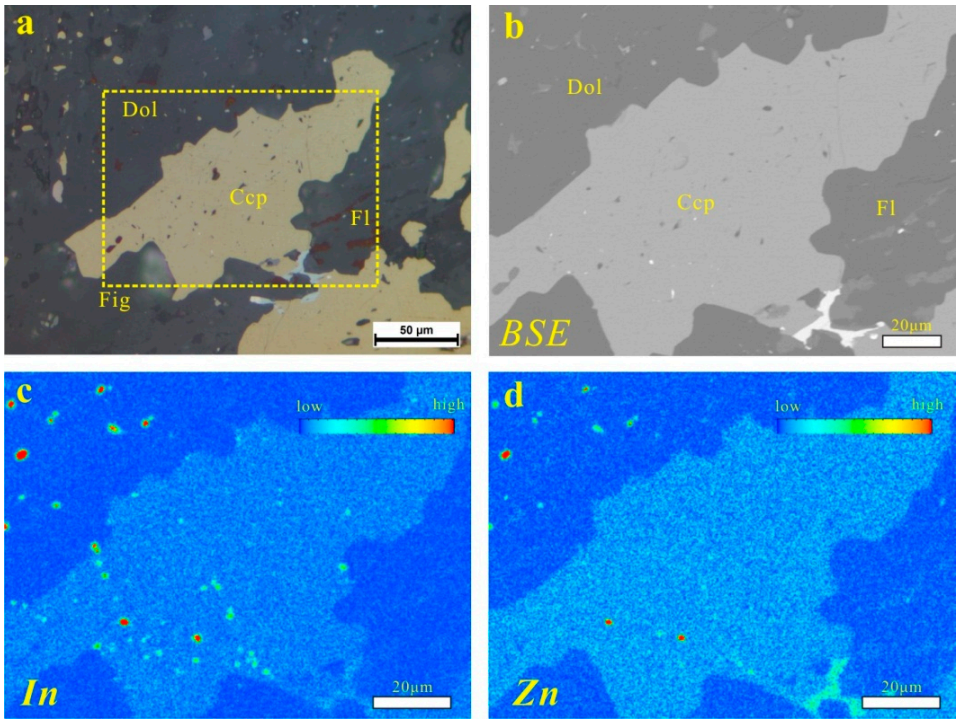

Figure 13. (**a**) Photomicrographs, (**b**) backscattered electron images, and X-ray element-distribution maps for (**c**) In and (**d**) Zn for chalcopyrite, showing that In and Zn are homogeneous in chalcopyrite except for the sphalerite inclusions.

4.2.3. Stannite

Stannite, a trace mineral, was observed in the type-I orebodies of the Tangguanpu and Paojinshan deposits and in the type-II orebodies of the Tangguanpu deposit. The EPMA data for stannite are listed in Table 5. The In content of the stannite from the type-I orebodies ranges from <0.02 to 3.68 wt %, while that in the stannite from the type-II orebodies ranges from <0.02 to 0.26 wt %. In addition, the stannite contains a small amount of Zn (0.83–5.00 wt %) and trace Cd (<0.03–0.25 wt %).

Table 5. EPMA data of stannite of the Xianghualing orefield (wt %).

Data	Zn	Fe	Cu	Sn	In	Cd	Mn	Ga	S	Total
Stannite in type-I orebodies, Tangguangpu deposit										
gy2a5	1.41	11.82	28.22	27.27	-	0.17	-	0.03	30.32	99.24
gy2a8'	0.83	12.81	29.13	27.10	-	0.14	-	-	30.58	100.59
gy2a9	0.83	12.91	28.84	27.51	-	0.07	-	-	30.32	100.48
gy2b1	1.13	12.66	28.91	25.33	0.31	0.25	-	-	30.00	98.59
gy2b2	1.02	12.42	29.03	26.45	0.17	0.19	-	-	30.21	99.49
gy2b3	1.30	12.73	29.08	26.31	0.06	0.22	-	-	30.46	100.16
gy5a4	1.98	11.60	29.43	27.06	0.03	0.06	-	-	30.09	100.25
gy5a5	2.27	12.04	29.45	26.76	-	0.04	-	-	30.19	100.75
gy5a6	1.96	12.30	28.70	26.07	-	0.04	-	-	29.96	99.03
Mean (9)	1.41	12.37	28.98	26.65	0.14	0.13	-	0.03	30.24	99.95
Stannite in type-I orebodies, Paojinshan deposit										
p4a1.3	2.87	11.47	27.72	26.49	0.14	0.05	-	0.03	30.03	98.80
p4a1.4	1.70	11.56	28.66	26.65	0.10	0.05	-	-	30.12	98.84
p4a1.5	1.79	11.94	28.91	26.80	0.11	0.03	-	-	30.11	99.69
p4a1.6	2.77	11.58	28.19	26.36	0.24	0.06	-	-	29.84	99.04
p4a1.7	1.55	11.52	28.35	26.82	0.14	0.06	-	-	29.60	98.04
p4b1.1	5.00	11.06	25.77	22.99	3.68	0.06	-	0.13	30.28	98.97
p4b1.2	4.13	11.60	26.53	23.25	3.41	0.07	-	0.13	30.06	99.18
p4c1.2	1.53	13.10	29.28	26.66	0.23	-	-	-	29.74	100.54
Mean (8)	2.67	11.73	27.93	25.75	1.01	0.05	-	0.10	29.97	99.14
Stannite in type-II orebodies, Tangguangpu deposit										
bb2b4	1.16	12.78	28.17	27.03	-	0.06	-	-	30.05	99.25
bb2b5	1.66	12.56	28.06	26.43	-	-	-	-	30.21	98.92
bb2b6	1.51	13.04	27.78	26.42	0.26	0.04	-	-	29.84	98.89
t21a8	4.80	11.60	27.43	25.14	0.13	0.06	-	-	30.28	99.44
t21a9	4.84	11.50	27.33	25.04	0.10	0.06	-	0.04	29.97	98.88
t21a10	3.15	11.73	28.42	25.61	0.07	0.06	-	-	29.78	98.82
t21a11	4.44	11.51	27.60	25.46	0.14	0.08	-	-	29.90	99.13
Mean (7)	3.08	12.10	27.83	25.88	0.14	0.06	-	0.04	30.00	99.05

"-" below detection limits.

5. Discussion

5.1. Indiumenriched Orebody Distribution in the Xianghualing Orefield

The type-I In-enriched Sn–Pb–Zn orebodies are controlled by both the faults and the intrusions in the orefield. The orebodies are located in the fault zone, are adjacent to the granites, and show ore zonation: (Sn→Sn–Pb–Zn→Pb–Zn–Sn→Pb–Zn mineralization from the proximal to the distal regions) [48,56,57], e.g., the Xinfeng and Paojinshan deposits. The major In-bearing orebodies are distributed along the NE trending F_1 and F_{101} faults and suborder faults. The In grade of the type-I orebodies of the four deposits studied varied dramatically. High In grade ores occur in the Tangguanpu and Paojinshan deposits; i.e., 1680 ppm and 620 ppm, respectively. The average In contents of type-I orebodies in the Xinfeng, Tangguanpu, Paojinshan, and Chashan deposits are 134 ppm, 376 ppm, 143 ppm and 328 ppm, respectively. The In contents of the type-I orebodies in the Xianghualing Orefield are higher than those of the skarn-type orebodies in the Yejiwei deposits in southern Hunan (avg. 114 ppm In, [24]). The vein-type orebodies in the Xianghualing Orefield are the richest In orebodies in southern Hunan. These type-II orebodies are controlled by the NE–EW trending granitic porphyry dikes. The In content of the type-II orebodies ranges from 10 to 152 ppm with an average of 64 ppm and is higher than that of the porphyry-type Sn orebodies (avg. 17 ppm In [24]) in the Yejiwei deposit in southern Hunan. Therefore, the two types of orebodies present in the Xianghualing ore system are significantly more enriched in In than other orebodies in southern Hunan. Despite have a geological setting similar to that of the other deposits in southern Hunan [30,38], the Xianghualing orefield is characterized as being suitable, having a magmatic-diapiric extensional structure [58].

The In-enriched vein and porphyry-type Sn–Pb–Zn orebodies were formed in normal faults and the associated suborder faults of the structure.

5.2. Indium Enriched Minerals in the Xianghualing Orefield

Discrete roquesite phenocrysts always occur in Zn-poor or zinc-free ores [4,10]. The ores in the two types of orebodies discussed are Zn-rich, and no roquesite was found in this study. Similar to most In-bearing deposits, In-bearing sphalerite is the most significant In-bearing mineral in the Xianghualing orefield. The EPMA data shows that sphalerite from the two types of orebodies contains variable In contents due to their locations and generation. In the type-I orebodies, the sphalerite from Sn ores contains a high In content, ranging from 2 to 8 wt % In and up to 21.96 wt % In on the rim of the sphalerite phenocrysts (Table 3). Sphalerite from Pb–Zn ores contains <0.10 wt % In. In the type-II orebodies, the sphalerite contains slightly higher In than that from the Pb–Zn ores of the type-I orebodies, e.g., sphalerite from disseminated ores contains 0.10–0.22 wt % In, and that from veinlet ores contains <0.02–0.39 wt % In. The chemical composition of the In-rich sphalerite from the Xianghualing orefield shows a positive correlation between In and Cu (Figure 11b) and the Sn content is very low, indicating cation replacement within the sphalerite: $(2Zn^{2+}) \leftrightarrow (Cu^{+}, In^{3+})$ [59]. Furthermore, the Cd content of the In-rich sphalerite ranges from 0.35–0.45 wt % Cd, showing characteristics of an "Indium window" in the Cu–In–S phase (Figure 16e) [55]. The In-bearing sphalerite contains chalcopyrite in solid solution (Figure 6a,b, and Figure 8d), which is similar to observation of other In deposits [14]. Chalcopyrite is a common and In-enriched mineral in In-bearing deposits [13,47]. The EPMA data shows that the chalcopyrite in the type-I orebodies contains <0.02–0.40 wt % In. The In contents of chalcopyrite and sphalerite are synchronously enriched. The In content of sphalerite from the Xinfeng and Paojinshan deposits is relatively high, and the In content of the chalcopyrite is also high. The In content of the sphalerite from the Chashan deposit is relatively low, and the In content of the chalcopyrite is also low. Stannite, a secondary mineral in the Sn–Pb–Zn deposits, consistently contains a small amount of In [4,13,24]. The type-I and type-II orebodies contain trace stannite. The EPMA data shows that the stannite contains <0.02–3.68 wt % In. Stannite from the type-I orebodies of the Paojinshan deposit contains higher In (<0.02–3.68 wt % In) than that of the type-II orebodies of the Tangguanpu deposit (<0.02–0.26 wt % In). Cassiterite, a major mineral in the In-rich Sn deposits, contains trace In, e.g., Sn-sulfide veins in far-eastern Russia contain 80–485 ppm In [54]. Unfortunately, the In line experiences interference from the Sn line during the EMPA analysis of cassiterite, so it is difficult to obtain an accurate In content for cassiterite [13]. Based on the mineral contents of ores and the In contents of thier minerals, sphalerite and chalcopyrite are the main In-enriched minerals in the Xianghualing orefield.

5.3. Genetic Considerations

The type-I orebodies of the Xianghualing orefield have been well-studied and exploited [48,50,56,57,60]. The $\delta^{34}S$ of the sulfides in the vein-type orebodies is −2.7‰–+6.7‰ [46] with an average of +2.5‰, indicating the sulfur is derived from magmatic rocks. The H–O isotopes of quartz in the ores indicates that the fluid of the early stage originated from magmatic water, while the isotopes of the later stages indicated added meteoric water [46]. Isotopic data for the type-I orebodies has not been obtained.

The biotite granite and granitic porphyry dikes, which are related to the vein and porphyry-type orebodies, respectively, are products of the same magma chamber. The petrology and geochemistry of the biotite granite indicates that it is an A-type granite [43]. The Xianghualing orefield is located in the northern Guangxi southern Hunan A-type granite belt [28,29]. Mineralization-related granitic intrusions in southern Hunan, e.g., the Qianlishan granite in the Shizhuyuan orefield [61] and granites in the Huangshaping deposit [36], formed during 160–150 Ma in a post-orogenic extensional and thinning tectonic environment [28,33]. The magmatic rocks originated from metasomatized Neoproterozoic volcanic-sedimentary materials [29,33] mixed with lithospheric-mantle-derived

magmas [28]. Important magmatic-hydrothermal In-bearing deposits around the world, e.g., Mount Pleasant in Canada [7], the Wiborg batholith in Finland [10,11], and the Freiberg district in Germany [14], are specific to A-type granites. The In content of the Laiziling intrusion ranges from 0.141 to 0.616 ppm (Liu Jianping, unpublished data), which is higher than the In content of the crust (0.05 ppm, [1]), indicating that the granites of the Xianghualing orefield are In-enriched. Furthermore, the granites of the Xianghualing Orefield contain high F (0.85–1.60 wt %, [43]). Ore minerals also include F- and B-bearing minerals, e.g., fluorite, topaz, and schorl. F and B play an important role during the mineralization of In and Sn [14]. Thus, the Xianghualing Orefield has a suitable intrusive magmatic setting for In mineralization.

In summary, the Xianghualing orefield has volatile-rich, In-rich A-type granites and normal faults in a magmatic-diaper extensional structural setting. These are two significant factors for the formation of the two types of In-enriched Sn–Pb–Zn orebodies.

6. Conclusions

Based on the geology, the petrology of the ores, the bulk chemistry of the ores, and the EPMA analysis of the two types of Sn–Pb–Zn orebodies in the Xianghualing orefield, the In mineralization features of the orefield can be summarized as follows:

(1) The Xianghualing orefield contains vein and porphyry-type Sn–Pb–Zn orebodies. The former occur in the main faults and are the most In-enriched orebodies, while the latter occur in the granitic porphyry dikes.

(2) Bulk chemical analysis of the ores shows the In content of the vein-type Sn–Pb–Zn orebodies varies from 0.79 to 1680 ppm (avg. 217 ppm, n = 29), and that of the porphyry-type orebodies varies from 10 to 150 ppm (avg. 64 ppm, n = 10).

(3) The EPMA data shows that sphalerite, chalcopyrite, and stannite are In-rich minerals, and sphalerite is the most significant In-rich mineral in the orefield. The most enriched sphalerite contains 7–8 wt % In in its core and up to 21.96 wt % In in its rim, which makes it the most In-enriched sphalerite in southern China. The Cd content of the In-rich sphalerite ranges from 0.35 to 0.45 wt % and exhibits an "Indium window" in the Cu-In-S phases.

(4) The In mineralization of the two types of In-bearing Sn–Pb–Zn orebodies was related to the intrusion of volatile-rich, In-rich, A-type granites and was controlled by normal faults within a magmatic-diapiric extensional structure.

Acknowledgments: This work was jointly supported by the National Natural Science Foundation of China (Grant 41302048) and the Innovation-driven Plan in Central South University (Grant 2015CX008).

Author Contributions: Jianping Liu, Yanan Rong, and Shugen Zhang conceived and designed the experiments; Zhongfa Liu, Jianping Liu and Weikang Chen performed the experiments; all authors wrote the paper.

Conflicts of Interest: The authors declare no conflict of interest.

References

1. Taylor, S.R.; McLennan, S.M. *The Continental Crust: Its Composition and Evolution*; Blackwell Scientific Publication: London, UK, 1985.
2. Tolcin, A.C. *Indium*; U.S. Geological Survey: Reston, VA, USA, 2013; pp. 35.1–35.5.
3. Chakhmouradian, A.R.; Smith, M.P.; Kynicky, J. From "strategic" tungsten to "green" neodymium: A century of critical metals at a glance. *Ore Geol. Rev.* **2015**, *64*, 455–458. [CrossRef]
4. Schwarz-Schampera, U.; Herzig, P.M. *Indium: Geology, Mineralogy, and Economics*; Springer: Berlin, Germany, 2002; pp. 1–257.
5. Ishihara, S.; Hoshino, K.; Murakami, H.; Endo, Y. Resource evaluation and some genetic aspects of indium in the Japanese ore deposits. *Resour. Geol.* **2006**, *56*, 347–364. [CrossRef]
6. Sinclair, W.D.; Kooiman, G.J.A.; Martin, D.A.; Kjarsgaard, I.M. Geology, geochemistry and mineralogy of indium resources at Mount Pleasant, New Brunswick, Canada. *Ore Geol. Rev.* **2006**, *28*, 123–145. [CrossRef]

7. Assadzadeh, G.E.; Samson, I.M.; Gagnon, J.E. Evidence for aqueous liquid-liquid immiscibility in highly evolved tin-bearing granites, Mount Pleasant, New Brunswick, Canada. *Chem. Geol.* **2017**, *448*, 123–136. [CrossRef]
8. Yang, X.M.; Lentz, D.R.; McCutcheon, S.R. Petrochemical evolution of subvolcanic granitoid intrusions within the Late Devonian Mount Pleasant Caldera, southwestern New Brunswick, Canada: Comparison of Au versus Sn-W-Mo-polymetallic mineralization systems. *Atlanta Geol.* **2003**, *39*, 97–121. [CrossRef]
9. Ishihara, S.; Murakami, H.; Marquez-Zavalia, M. Inferred indium resources of the Bolivian tin-polymetallic deposits. *Resour. Geol.* **2011**, *61*, 174–191. [CrossRef]
10. Cook, N.J.; Sundblad, K.; Valkama, M.; Nygård, R.; Ciobanu, C.L.; Danyushevsky, L. Indium mineralization in A-type granites in southeastern Finland: Insights into mineralogy and partitioning between coexisting minerals. *Chem. Geol.* **2011**, *284*, 62–73. [CrossRef]
11. Valkama, M.; Sundblad, K.; Nygård, R.; Nigel, C. Mineralogy and geochemistry of indium-bearing polymetallic veins in the Sarvlaxviken area, Lovisa, Finland. *Ore Geol. Rev.* **2016**, *75*, 206–219. [CrossRef]
12. Valkama, M.; Sundblad, K.; Cook, N.J.; Ivashchenko, V.I. Geochemistry and petrology of the indium-bearing polymetallic skarn ores at Pitkäranta, Ladoga Karelia, Russia. *Miner. Depos.* **2016**, *51*, 823–839. [CrossRef]
13. Andersen, J.C.Ø.; Stickland, R.J.; Rollinson, G.K.; Shail, R.K. Indium mineralization in SW England: Host parageneses and mineralogical relations. *Ore Geol. Rev.* **2016**, *78*, 213–238. [CrossRef]
14. Seifert, T.; Sandmann, D. Mineralogy and geochemistry of indium-bearing polymetallic vein-type deposits: Implications for host minerals from the Freiberg district, Eastern Erzgebirge, Germany. *Ore Geol. Rev.* **2006**, *28*, 1–31. [CrossRef]
15. Oliveira, D.; Matos, J.; Rosa, C.; Rosa, D.; Figueiredo, M.; Silva, T.; Guimaraes, F.; Carvalho, J.; Pinto, A.; Relvas, J.; Reiser, F. The LagoaSalgada orebody, Iberian Pyrite Belt, Portugal. *Econ. Geol.* **2011**, *106*, 1111–1128. [CrossRef]
16. Oliveira, D.; Rosa, D.; Figueiredo, M. Renewable energy technologies for the 21st century: The Iberian Pyrite Belt as a possible supplier of indium. In Proceedings of the 9th Biennial SGA Meeting of the Society for Geology Applied to Mineral Deposits Meeting, Dublin, Ireland, 20–23 August 2007; pp. 1263–1266.
17. Ishihara, S.; Endo, Y. Indium and other trace elements in volcanogenic massive sulfide ores from the Kuro, Besshi and other types in Japan. *Bull. Geol. Surv. Jpn.* **2007**, *58*, 7–22. [CrossRef]
18. Zhang, Q.; Zhu, X.; He, Y.; Jiang, J.; Wang, D. Indium enrichment with Meng'entaolegai Ag–Pb–Zn deposit, Inner Mongolia, China. *Resour. Geol.* **2006**, *56*, 337–346. [CrossRef]
19. Ishihara, S.; Qin, K.; Wang, Y. Resource evaluation of indium in the Dajing tin-polymetallic deposits, Inner Mongolia, China. *Resour. Geol.* **2008**, *58*, 72–79. [CrossRef]
20. Ishihara, S.; Murakami, H.; Li, X. Indium concentration in zinc ores in plutonic and volcanic environments: Examples at the Dulong and Dachang mines, South China. *Bull. Geol. Surv. Jpn.* **2011**, *62*, 259–272. [CrossRef]
21. Pi, Q.; Hu, R.; Wang, D.; Miao, D.; Qin, X.; Chen, H. Enrichment of indium in west ore belt of Dachang orefield: Evidence from ore textures and sphalerite geochemistry. *Miner. Depos.* **2015**, *34*, 379–396. (In Chinese)
22. Cheng, Y. Occurrence characteristics and enrichment regularity of indium in pyrite: A case study of Dachang tin ore-field. *Trans. Nonferrous Met. Soc. China* **2016**, *26*, 2197–2208. [CrossRef]
23. Liu, J. Indium mineralization in a Sn-poor skarn deposit: A case study of the Qibaoshan deposit, South China. *Minerals* **2017**, *7*, 76. [CrossRef]
24. Liu, J.; Rong, Y.; Gu, X.; Shao, Y.; Lai, J.; Chen, W. Indium mineralization in the Yejiwei Sn-polymetallic deposit of the Shizhuyuan Orefield, southern Hunan, China. *Resour. Geol.* **2017**, *67*. in press.
25. Che, Q.; Li, J.; Wei, S.; Wu, G. Elementary discussion on the tectonic background of deposit-concentrated Qianlishan-Qitianling area in Hunan. *Geotect. Met.* **2005**, *29*, 204–214. (In Chinese)
26. Wang, Y.; Zhu, J.; Yu, Q. *Geology of Lead-Zinc Deposits in Hunan Province*; Geological Publishing House: Beijing, China, 1988. (In Chinese)
27. Wang, X.; Wang, W. *Geology of the Xianghualing Non-Ferrous and Rare Metals Polymetallic Deposits, Hunan*; Bureau of Geological Prospecting of China Nonferrous Metals Industry Corporation: Beijing, China, 1997; pp. 1–76. (In Chinese)
28. Jiang, S.; Zhao, K.; Jiang, Y.; Dai, B. Characteristics and genesis of Mesozoic A-type granites and associated mineral deposits in the southern Hunan and northern Guangxi provinces along the Shi-Hang belt, south China. *Geol. J. China Univ.* **2008**, *14*, 496–509. (In Chinese)
29. Zhu, J.; Chen, J.; Wang, R.; Lu, J.; Xie, L. Early Yanshanian NE trending Sn/W-bearing A-type granites in the western-middle part of the Nanling Mts region. *Geol. J. China Univ.* **2008**, *14*, 474–484. (In Chinese)

30. Peng, J.; Zhou, M.; Hu, R.; Shen, N.; Yuan, S.; Bi, X.; Du, A.; Qu, W. Precise molybdenite Re–Os and mica Ar–Ar dating of the Mesozoic Yaogangxian tungsten deposit, central Nanling district, South China. *Miner. Deposita* **2006**, *41*, 661–669. [CrossRef]
31. Zhu, J.; Wang, R.; Zhang, P.; Xie, C.; Zhang, W.; Zhao, K.; Xie, L.; Yang, C.; Che, X.; Yu, A.; Wang, L. Zircon U–Pb geochronological framework of Qitianling granite batholith, middle part of Nanling Range, South China. *Sci. China Ser. D* **2009**, *52*, 1279–1294. [CrossRef]
32. Xie, L.; Wang, R.; Chen, J.; Zhu, J. Mineralogical evidence for magmatic and hydrothermal processes in the Qitianling oxidized tin-bearing granite (Hunan, South China): EMP and (MC)-LA-ICPMS investigations of three types of titanite. *Chem. Geol.* **2010**, *276*, 53–68. [CrossRef]
33. Shu, X.; Wang, X.; Sun, T.; Xu, X.; Dai, M. Trace elements, U–Pb ages and Hf isotopes of zircons from Mesozoic granites in the western Nanling Range, South China: Implications for petrogenesis and W–Sn mineralization. *Lithos* **2011**, *127*, 468–482. [CrossRef]
34. Mao, J.; Cheng, Y.; Chen, M.; Pirajno, F. Major types and time–space distribution of Mesozoic ore deposits in South China and their geodynamic settings. *Miner. Deposita* **2013**, *48*, 267–294.
35. Ding, T.; Ma, D.; Lu, J.; Zhang, R. Apatite in granitoids related to polymetallic mineral deposits in southeastern Hunan Province, Shi–Hang zone, China: Implications for petrogenesis and metallogenesis. *Ore Geol. Rev.* **2015**, *69*, 104–117. [CrossRef]
36. Li, H.; Watanabe, K.; Yonezu, K. Geochemistry of A-type granites in the Huangshaping polymetallic deposit (South Hunan, China): Implications for granite evolution and associated mineralization. *J. Asian Earth Sci.* **2014**, *88*, 149–167. [CrossRef]
37. Ding, T.; Ma, D.; Lu, J.; Zhang, R.; Zhang, S. S, Pb, and Sr isotope geochemistry and genesis of Pb–Zn mineralization in the Huangshaping polymetallic ore deposit of southern Hunan Province, China. *Ore Geol. Rev.* **2016**, *77*, 117–132. [CrossRef]
38. Li, X.; Huang, C.; Wang, C.; Wang, L. Genesis of the Huangshaping W–Mo–Cu–Pb–Zn polymetallic deposit in southeastern Hunan Province, China: Constraints from fluid inclusions, trace elements, and isotopes. *Ore Geol. Rev.* **2016**, *79*, 1–25.
39. Yuan, S.; Peng, J.; Hu, R.; Li, H.; Shen, N.; Zhang, D. A precise U–Pb age on cassiterite from the Xianghualing tin-polymetallic deposit (Hunan, South China). *Miner. Deposita* **2008**, *43*, 375–382. [CrossRef]
40. Yuan, S.; Peng, J.; Hao, S.; Li, H.; Geng, J.; Zhang, D. In situ LA-MC-ICP-MS and ID-TIMS U–Pb geochronology of cassiterite in the giant Furong tin deposit, Hunan Province, South China: New constraints on the timing of tin–polymetallic mineralization. *Ore Geol. Rev.* **2011**, *43*, 235–242. [CrossRef]
41. Cai, H. The metallogenic geological setting and approach on ore genesis of the Xianghualing tin-polymetallic ore field. *Miner. Resour. Geol.* **1991**, *5*, 272–283. (In Chinese)
42. Lei, Z.; Xu, Y.; Hu, Z. Analyse prospects of Jijiaoshan tungsten polymetallic deposit of Linwu County, Hunan Province. *Geol. Miner. Resour. South China* **2008**, *4*, 36–42. (In Chinese)
43. Zhu, J.; Wang, R.; Zhang, H.; Zhang, W.; Xie, L.; Zhang, R. Fractionation, evolution, petrogenesis and mineralization of Laiziling granite pluton, southern Hunan province. *Geol. J. China Univ.* **2011**, *17*, 381–392. (In Chinese)
44. Du, S.; Qiu, R. A preliminary study on the evolutionary characteristics of rare earth elements (REE) in granitoid rocks and their formation mechanisms in Xianghualing region, Hunan Province, China. *Chin. J. Geochem.* **1991**, *10*, 68–79.
45. Xu, Q. Identification of the intrusive phases of the composite alkali-feldspathic granite in Xianghualing, Hunan. *Hunan Geol.* **1991**, *10*, 289–294. (In Chinese)
46. Lai, S. Research on Mineralization of the Xianghualing Tin-Polymetallic Deposit, Hunan, China. Ph.D. Thesis, China University of Geosciences (Beijing), Beijing, China, 2014. (In Chinese)
47. Briskey, J.A. *Indium in Zinc-Lead and Other Mineral Deposits*; U.S. Geological Survey: Reston, VA, USA, 2005; pp. 1–8.
48. Wen, G.; Guo, L.; Ding, C. Preliminary study on mineralization zonation of Xianghualing tin–lead–zinc polymetallic deposit, Liwu County. *Hunan Geol.* **1984**, *3*, 18–29. (In Chinese)
49. Zou, T. Geological characteristics and genesis of granitic porphyry-type tin-polymetallic deposit. In *Geological Prospecting and Mineral Economy in China*; Sun, Z.J., Ed.; Central South University Press: Changsha, China, 2000; pp. 224–231. (In Chinese)

50. Zhang, D.; Wang, L. Metallogenic zoning and genesis of the Xianghualing orefield. *Miner. Depos.* **1988**, *7*, 35–44. (In Chinese)
51. Hu, Y.; Huang, R.; Gong, M. Two metal mineralization series endogentic lead–zinc deposits in South Hunan. *Hunan Geol.* **1984**, *3*, 5–17. (In Chinese)
52. Zhong, J.; Li, C. Geological characteristics and genesis of Xianghualing skarn type tin deposit. *Miner. Resour. Geol.* **2006**, *20*, 147–151. (In Chinese)
53. Benzaazoua, M.; Marion, P.; Pinto, A.; Migeon, H.; Wagner, F.E. Tin and indium mineralogy within selected samples from the Neves Corvo ore deposit (Portugal): A multidisciplinary study. *Miner. Eng.* **2003**, *16*, 1291–1302. [CrossRef]
54. Pavlova, G.G.; Palessky, S.V.; Borisenko, A.S.; Vladimirov, A.G.; Seifert, T.; Phan, L.A. Indium in cassiterite and ores of tin deposits. *Ore Geol. Rev.* **2015**, *66*, 99–113. [CrossRef]
55. Dill, H.G.; Garrido, M.M.; Melcher, F.; Gomez, M.C.; Weber, B.; Luna, L.I.; Bahr, A. Sulfidic and non-sulfidic indium mineralization of the epithermal Au–Cu–Zn–Pb–Ag deposit San Roque (Provincia Rio Negro, SE Argentina)—With special reference to the "indium window" in zinc sulfide. *Ore Geol. Rev.* **2013**, *51*, 103–128. [CrossRef]
56. Wen, G.; Li, H.; Li, S. The genesis of Chashan Pb–Zn deposit of Linwu County. *Hunan Geol.* **1988**, *7*, 40–47. (In Chinese)
57. Wen, G.; Wu, Q. The ore-controlling factors and genesis of Paojinshan Pb–Zn deposit, Linwu, Hunan. *J. Guilin Inst. Technol.* **1990**, *10*, 356–363. (In Chinese)
58. Wang, Y.; Duan, J.; Zhou, C. The magmatic-diapiric extensional tectonics of Xianghualing Hunan. *Miner. Resour. Geol.* **1994**, *8*, 88–92. (In Chinese)
59. Murakami, H.; Ishihara, S. Trace elements of indium-bearing sphalerite from tin-polymetallic deposits in Bolivia, China and Japan: A femto-second LA-ICPMS study. *Ore Geol. Rev.* **2013**, *53*, 223–243. [CrossRef]
60. Zhou, T.; Liu, W.; Li, H.; Xu, W.; Dai, T. Isotope geochemistry of the Xianghualing tin-polymetallic deposit in Hunan Province. *Acta Geosci. Sin.* **2008**, *29*, 703–708. (In Chinese)
61. Chen, Y.; He, L.; Sun, W.; Ireland, T.; Tian, X.; Hu, Y.; Yang, W.; Chen, C.; Xu, D. Generation of Late Mesozoic Qianlishan A_2-type granite in Nanling Range, South China: Implications for Shizhuyuan W–Sn mineralization and tectonic evolution. *Lithos* **2016**, 266–277, 435–452. [CrossRef]